

Published in final edited form as:

Nature. 2019 May ; 569(7756): 418–422. doi:10.1038/s41586-019-1191-6.

## MicroRNA therapy stimulates uncontrolled cardiac repair after myocardial infarction in pigs

Khatia Gabisonia<sup>1,#</sup>, Giulia Prosdocimo<sup>2,#</sup>, Giovanni Donato Aquaro<sup>3,#</sup>, Lucia Carlucci<sup>1</sup>, Lorena Zentilin<sup>2</sup>, Ilaria Secco<sup>2,4</sup>, Hashim Ali<sup>2,4</sup>, Luca Braga<sup>2,4</sup>, Nikoloz Gorgodze<sup>1</sup>, Fabio Bernini<sup>1</sup>, Silvia Burchielli<sup>3</sup>, Chiara Collesi<sup>2,5</sup>, Lorenzo Zandonà<sup>5</sup>, Gianfranco Sinagra<sup>5</sup>, Marcello Piacenti<sup>3</sup>, Serena Zacchigna<sup>5,6</sup>, Rossana Bussani<sup>5</sup>, Fabio A. Recchia<sup>1,3,7,\*</sup>, Mauro Giacca<sup>2,4,5,\*</sup>

<sup>1</sup>Institute of Life Sciences, Scuola Superiore Sant'Anna, 56127 Pisa, Italy

<sup>2</sup>Molecular Medicine Laboratory, International Centre for Genetic Engineering and Biotechnology (ICGEB), 34149 Trieste, Italy

<sup>3</sup>Fondazione Toscana “Gabriele Monasterio”, 56124 Pisa, Italy

<sup>4</sup>School of Cardiovascular Medicine & Sciences, King's College London, London SE5 9N

<sup>5</sup>Department of Medical, Surgical and Health Sciences, University of Trieste, 34127 Trieste, Italy

<sup>6</sup>Cardiovascular Biology Laboratory, International Centre for Genetic Engineering and Biotechnology (ICGEB), 34149 Trieste, Italy

<sup>7</sup>Cardiovascular Research Center, Lewis Katz School of Medicine at Temple University, Philadelphia 19140, USA

### Abstract

Prompt coronary catheterization and revascularization have dramatically improved the outcome of myocardial infarction, but also have resulted in a growing number of survived patients with permanent structural damage of the heart, which frequently leads to heart failure. Finding new treatments for this condition is a largely unmet clinical need 1, especially because of the incapacity of cardiomyocytes to replicate after birth and thus achieve regeneration of the lost contractile tissue 2. Here we show that expression of human microRNA-199a in infarcted pig hearts is

---

Users may view, print, copy, and download text and data-mine the content in such documents, for the purposes of academic research, subject always to the full Conditions of use:[http://www.nature.com/authors/editorial\\_policies/license.html#terms](http://www.nature.com/authors/editorial_policies/license.html#terms)

**Correspondence and requests for materials** should be addressed to M.G. or F.A.R.: Mauro Giacca, MD PhD, ICGEB, Padriciano, 99, 34149 Trieste, Italy, tel.: +39 040 375 7324, [giacca@icgeb.org](mailto:giacca@icgeb.org); Fabio A. Recchia, MD PhD, Institute of Life Sciences, Scuola Superiore Sant'Anna, 56100 Pisa, Italy, Phone: +39 050 883266, [fabio.recchia@santannapisa.it](mailto:fabio.recchia@santannapisa.it).

<sup>#</sup>Contributed equally to the work as first authors

<sup>\*</sup>Both authors contributed as senior authors

#### Data availability

All relevant data are included in the paper and its Extended Data information.

**Author Contributions.** MG and FAR designed the experiments and supervised the project. KG, LC, NG, FB and SB performed the in vivo pig experimentation. GDA performed cMRI and analysis of cMRI images. GP, IS, HA, LB and CC performed molecular and immunofluorescence analysis. RB and LZ performed histological and immunohistochemistry analysis. SZ provided essential advice for the experimental design. LZ supervised production of AAV vectors. MP and GS provided expert advice on electrophysiology and heart failure studies.

**Competing interests.** The authors declare no competing interests.

capable of stimulating cardiac repair. One month after myocardial infarction and delivery of this microRNA through an adeno-associated viral vector, the treated animals showed marked improvements in both global and regional contractility, increased muscle mass and reduced scar size. These functional and morphological findings correlated with cardiomyocyte de-differentiation and proliferation. At longer follow-up, however, persistent and uncontrolled expression of the microRNA resulted in sudden arrhythmic death of most of the treated pigs. Such events were concurrent with myocardial infiltration of proliferating cells displaying a poorly differentiated myoblastic phenotype. These results show that achieving cardiac repair through the stimulation of endogenous cardiomyocyte proliferation is attainable in large mammals, however this therapy needs to be tightly dosed.

---

The neonatal mammalian heart immediately after birth 3 and the heart of urodeles and fish during their entire life 4,5 are capable of spontaneous regeneration. In these cases, new tissue formation occurs through the partial de-differentiation of already existing cardiomyocytes (CMs), followed by their proliferation 3,6,7. In adult mammals, instead, CM proliferation is only marginally increased after myocardial infarction (MI) 8, but remains far below clinically significant levels. Thus, empowering the endogenous capacity of CM proliferation after damage remains an exciting strategy to achieve cardiac repair.

Past work has shown that CM proliferation is under the control of the microRNA (miRNA) network 9–12. In particular, high throughput screening work from our laboratory revealed that a few human miRNAs, including hsa-miR-199a-3p, can stimulate rodent CM entry into the cell cycle and cardiac regeneration after MI in mice 11. We thus wanted to explore whether these findings could be translated in porcine MI, a clinically relevant large animal model.

We identified AAV serotype 6 (AAV6) as the most effective vector to transduce pig cardiomyocytes after intramyocardial injection (Extended Data Figs. 1a and 1b). Then, we generated an AAV6 vector expressing the hsa-miR-199a-1 pri-miRNA gene under the control of the constitutive CMV promoter; the sequences of both miR-199a-3p and miR-199a-5p, produced from this pri-miRNA, are identical in rats, mice, pigs and humans (Extended Data Figs. 1c and 1d). MI was induced in 25 pigs by 90-minute occlusion of the left anterior coronary artery followed by reperfusion. Animals were randomly divided into 2 groups receiving either  $2 \times 10^{13}$  empty AAV6 (AAV6-Control) particles or the same dose of AAV6-miR-199a (Fig. 1a and Extended Data Fig. 1e) injected into in the left ventricle (LV) wall. An additional group of sham operated animals served as control. The levels of transduction and transgene expression were robust and persistent over time in the injected areas, as assessed by both quantitative PCR and in situ hybridisation (Figs. 1b and 1c; Extended Data Fig. 2). Both miRNA strands were expressed at comparable levels (Extended Data Fig. 3a). We also verified that a few of the known miR-199a targets were effectively downregulated in the treated animals. These included two factors in the Hippo pathway (the upstream inhibitory TAO kinase1, TAOK1 13,14) and the phospho-YAP E3 ubiquitin-ligase  $\beta$ -transducing repeat containing protein,  $\beta$ -TrCP 15) and the actin cytoskeleton regulatory protein Cofilin2 16 for miR-199a-3p, in addition to HIF1 for miR-199a-5p 17 (Extended Data Fig. 3b). Target sites for these miRNAs are conserved in swine (Extended Data Figs.

3c-f). Viral DNA spread and levels of transgene miR-199a expression remained essentially restricted to the injected myocardium (Extended Data Figs. 3g and 3h).

Morphological and functional assessment was performed using cardiac magnetic resonance imaging (cMRI) based on gadolinium delayed contrast-enhanced images (late gadolinium enhancement, LGE). At 2 days post-MI, the gadolinium-retaining region, defined as either infarct mass or size, was not significantly different between the AAV6-Control and AAV6-miR-199a groups ( $n=12$  and  $13$  respectively), in agreement with the measurements of oedema extension based on enhanced T2-weighted signals 18 (Figs. 1d and 1e). At 4 weeks post-MI, instead, both scar mass and size resulted approximately 50% reduced in the AAV6-miR-199a-treated animals (Figs. 1f for mean results and Extended Data Fig. 4a for paired analyses in the same animals).

Representative LGE-cMRI images of 5 cross-sectional planes (a-e, Fig. 1g) of hearts from two representative animals per group at days 2 and 28 after MI are shown in Fig. 1h. A marked reduction in scar size (identified by red counterstain) at day 28 is appreciable in the animals that received AAV6-miR-199a (the original images without counterstain are in Extended Data Fig. 4b). For two other representative animals, gross anatomy of cardiac slices with corresponding LGE-MR images at day 28 are shown in Extended Data Fig. 4c. Concordant with the cMRI data, the fibrotic area in the infarcted region was significantly reduced at 28 days (Figs. 1i and 1j). The infarct region included a core fibrotic area and a surrounding grey zone, composed of a mixture of viable myocardium and fibrotic regions (Fig. 1k). At 28 days post-MI, the core was smaller in the AAV6-miR-199a group ( $P<0.05$ ; Fig. 1l), also suggestive of a process of regeneration driven by miR-199a in the infarct border zone.

Functional data measured by cMRI showed that LV ejection fraction was recovered at 28 days in the animals injected with AAV6-miR-199a, while it remained more than 20 points below sham values in AAV6-Control ( $P<0.05$ ; Fig. 2a). Similarly, LV stroke volume at day 28 in AAV6-miR-199a-treated animals returned to levels similar to those of sham pigs (Fig. 2b). This was mainly due to the partial recovery of the LV end-systolic volume in the AAV6-miR-199a group, while LV end-diastolic volume was not changed (Figs. 2c and 2d). cMRI short axis videos of two infarcted animals, treated with either AAV6-Control or AAV6-miR-199a, are shown in Suppl. Video 1. There was no significant difference in heart rate among the animals (Extended Data Fig. 4d).

In addition to global cardiac function, cMRI was also used to assess regional/segmental contractility using MRI-tagging (Fig. 2e). Radial strain ( $E_{RR}$ ) and circumferential strain ( $E_{CC}$ ) were evaluated along short-axis LV slices (basal, middle, and apical) divided into 8 equal circumferential segments (Fig. 2f). Values for each segment were plotted to generate curves (Fig. 2g and 2h); the area under the curve (AUC 19,20) was then calculated (scheme in Fig. 2i). This segmental analysis revealed significant recovery of both  $E_{RR}$  and  $E_{CC}$  in the AAV6-miR-199a group at 28 days after MI (Figs. 2j and 2k). Analysis of systolic LV wall thickening yielded similar results (Figs. 2l and 2m).

Morphological and functional improvement correlated with increased CM proliferation. In the infarct border zone of AAV6-miR-199a-treated pigs (n=5 per group) injected with BrdU from day 2 to day 12 (Fig. 3a), there was an increase in the number of CMs positive for Ki67 (a proliferation marker; Fig. 3b and Extended Data Fig. 5a), or incorporating BrdU (an S-phase marker; Fig. 3c) or containing phosphorylated histone H3 (pH3, a marker of transition through G2/M; Fig. 3d and Extended Data Fig. 5b). More occasionally, CMs showed Aurora B kinase localization in midbodies, marking cells undergoing cytokinesis (Fig. 3e). Replicating cardiomyocytes were mono- or bi-nucleated (Figs. 3f and 3g and Extended Data Figs. 6a and 6b), in spite of the heavily multinucleated nature of swine CMs<sup>21</sup>. There were no differences in either distribution of multi-nucleated fibres between treated and control animals or cross-sectional area between BrdU-positive and BrdU-negative CMs (Extended Data Figs. 6c and 6d). Collectively, these results show that expression of miR-199a boosts endogenous CM proliferation. Of interest, proliferation occurred in cells that remained connected to one another via intact connexin-43 (CX43) desmosomes at intercalated discs, consistent of electrical integration (Fig. 3h).

In the infarct border zone, where AAV6-miR-199a had been injected, a number of cells with CM morphology expressed GATA4 (Figs. 3i and 3j), a transcription factor essential for cardiac development<sup>22</sup> and re-expressed during zebrafish heart regeneration<sup>7</sup>. GATA4 normally localizes in the nucleus where it promotes transcription of cardiac genes, but is also found in the cytoplasm during embryonic development<sup>23</sup>. Presence of these cells persisted at 28 days and was restricted to the injected infarct border (Extended Data Fig. 7).

We explored some of the molecular correlates of cardiac repair and improved cardiac function. The ratio between transcripts for adult  $\alpha$ - and foetal  $\beta$ -myosin heavy chains was maintained by AAV6-miR-199a (Extended Data Fig. 8a). A trend towards preservation from maladaptive hypertrophy by miR-199a was observed at 30 days both macroscopically post-mortem (Extended Data Fig. 8b) and by quantifying CM sectional area (Extended Data Fig. 8c and 8d). Consistently, increase in both atrial and brain natriuretic peptide (ANP and BNP) gene expression was blunted in the AAV6-miR-199a-treated animals (Extended Data Figs. 8e and 8f respectively). There were no significant differences in the levels of pathological muscle and vascular markers in the miR-199a-treated animals, including desmin, myogenin, endothelin-B receptor and Wt1 (Extended Data Fig. 8g). Finally, no difference in vessel density was detected (Extended Data Fig. 8h).

A subset of infarcted animals treated with AAV6-Control (n=9) and AAV6-miR-199a (n=10) was followed beyond the first month from treatment. Three of the AAV6-miR-199a pigs continued to show persistent beneficial effects on cardiac morphology and function at 8 weeks, with progressive reduction of cardiac scar (Fig. 4a and Extended Data Fig. 9a). cMRI images over time of a second pig, along with gross cardiac morphology after euthanasia at 2 months, are shown in Extended Data Figs. 9b and 9c). Despite this progressive morpho-functional improvement until seemingly complete restoration, 7 out of 10 pigs in the AAV6-miR-199a group died from sudden death at weeks 7-8, in the absence of preceding clinical signs (Fig. 4b). In two of these pigs, a subcutaneously implanted miniaturized recorder documented the final phases of ECG preceding sudden death, showing tachyarrhythmia events that had evolved into ventricular fibrillation (Extended Data Figs. 10a and 10b). The

mRNA levels of 14 different ion channels or associated proteins involved in various types of arrhythmogenic conditions did not reveal significant differences between miR-199a-treated and control animals, which was against the possibility that miR-199a might directly affect channels controlling cardiac electric activity (Extended Data Figs. 10c). Thus, these tachyarrhythmias might be consequent to the generation of areas of poorly-differentiated CMs that, by progressively growing in size, eventually determine fatal re-entry electric circuits. Alternatively, they might arise because of the simultaneous expression, from the same vector and in addition to pro-regenerative miR-199a-3p, also of the miR-199a-5p strand, which is known to exert deleterious effects in the heart 24–27.

Examination of haematoxylin-eosin-stained tissue sections from AAV6-miR-199a-injected pigs revealed the occasional presence of small clusters of cells infiltrating the myocardium (Fig. 4c and Extended Data Fig. 11). These cells were negative for markers of inflammatory (CD45) or hematopoietic and endothelial (CD34) cells, or for markers identifying differentiated muscle (desmin, sarcomeric  $\alpha$ -actinin, HHF35) or epicardial (Wt1) cells. They were proliferating (positive for Ki67) and expressed a few antigens present during early myogenic development, including GATA4, myogenin (the reactivation of which characterizes rhabdomyosarcoma cells), caldesmon (expressed at high levels in leiomyoma and leiomyosarcoma) and the endothelin-B receptor (expressed in smooth muscle cells). Of note, in situ hybridisation revealed that these clusters were negative for miR-199a while being surrounded by CMs expressing this miRNA (Fig. 4d). Thus, these cells had either lost the AAV6 vectors due to their replication (AAVs do not integrate into the host cell genome 28) or they arose as a consequence of an altered microenvironment induced by AAV6-miR-199a-expressing CMs.

The use of miRNAs as genetic tools to stimulate cardiac proliferation is appealing, as it leverages the capacity of these molecules to regulate the levels of multiple genes simultaneously. Our study indeed shows that cardiac AAV6-miR-199a delivery reduces infarct size, diminishes cardiac fibrosis and improves contractile function in infarcted pigs by stimulating CM de-differentiation and proliferation. However, uncontrolled, long-term expression of this miRNA eventually determined sudden cardiac death of most animals. Therefore, cardiac administration of pro-proliferative miRNAs can stimulate cardiac repair after MI but needs to be properly dosed. This is currently beyond the properties of virus-mediated gene transfer but can be achieved through cardiac delivery of naked, synthetic miRNA mimics 29.

## Methods

### Production and purification of recombinant AAV vectors

Hsa-miR-199a was amplified from human genomic DNA isolated from HeLa cells, using the QIAamp DNA mini kit (Qiagen), according to the manufacturer's instructions, as previously described 11. The amplified sequence was cloned into the pZac2.1 vector (Gene Therapy Program, Penn Vector core, University of Pennsylvania, USA), which was used to produce recombinant AAV vectors in the AAV Vector Unit at ICGEB Trieste, as described previously 30. In particular, AAV serotype 6 vectors were generated in HEK293T cells, by

co-transfecting the plasmid vector together with the packaging plasmid pDP6 (PlasmidFactory, Germany).

Viral stocks were obtained by PEG precipitation and two subsequent CsCl<sub>2</sub> gradient centrifugations. Titration of AAV viral particles was performed by real-time PCR quantification of the number of packaged viral genomes, as described previously 31; the viral preparations had titres between  $1.3 \times 10^{13}$  and  $3.3 \times 10^{13}$  viral genomes per ml.

### Open chest surgery and myocardial infarction

Three- to four-month old male farm pigs, weighting 28-32 kg, were sedated with a cocktail of 4 mg/kg tiletamine hydrochloride and 4 mg/kg zolazepam hydrochloride injected intramuscularly, intubated and mechanically ventilated with positive pressure. Inhalatory anaesthesia was maintained by a mixture of 1-2% isoflurane dissolved in 40% air and 60% oxygen. Electrocardiogram (ECG), heart rate and arterial pressure were constantly monitored. A thoracotomy was performed in the left fourth intercostal space and then the pericardial sac was opened to expose the heart. A small group of animals (n=3) received direct intramyocardial injections of  $1 \times 10^{12}$  v.g. AAV6, AAV8 and AAV9, suspended in PBS and carrying the reporter gene eGFP, in 3 separate sites of the LV anterior wall, one vector serotype for each site, to compare their transduction efficiency.

Myocardial infarction (MI) was induced by coronary occlusion in 19 pigs anesthetized and operated as described above. Thirty min before coronary occlusion, pigs were medicated with 4.3 mg/kg of amiodarone in 500 ml of 0.9% sodium chloride to prevent arrhythmias. The left anterior descending coronary artery (LAD) was isolated from surrounding tissue distal to the first diagonal branch, encircled by a suture thread (Extended Data Fig. 1e); the two ends of the suture were threaded through a plastic tube and tightened to achieve occlusion of the vessel, confirmed by the presence of regional myocardial cyanosis, ST segment elevation in the ECG and ventricular arrhythmias, which were more pronounced within the first 30-45 min. The LAD occlusion was removed after 90 min to start the reperfusion phase.

After 10 min of reperfusion, the survived animals were randomized in 2 groups receiving:  $2 \times 10^{13}$  empty AAV6 (AAV6-control; n=12) or  $2 \times 10^{13}$  AAV6-hsa-miR-199a-3p (AAV6-miR-199a; n=13). The viral particles were suspended in 2 ml of PBS and delivered by 20 direct intramyocardial injections equally spaced along the border zone (100  $\mu$ l per injection). The latter was visually identified as the margin of the ischemic myocardium (pale compared to the normally perfused myocardium; Extended Data Fig. 1e). Some of the injection sites were tagged with coloured epicardial stitches to detect and sample the corresponding myocardial tissue post-mortem for histological analysis. An additional group of sham-operated animals was operated in the same manner, but LAD was not ligated (sham; n=6). In this experimental setting, the delivery of the vector at the time of MI allows avoiding a second surgery a few days/hours after MI, which would importantly increase animal mortality.

At the end of the study, animals were anaesthetized and sacrificed by injection of 10% KCl to stop the heart at diastole. The excised hearts were sectioned through four horizontal



planes and each section was then subdivided into sub-sections for further histological and molecular analysis as shown in Extended Data Figs. 2a and 2b. Briefly, each heart was sectioned in four 1-cm thick slices, starting from the apex towards the base. Then, each slice was divided into 2-8 regions (indicated by letters). In all quantifications, we have considered at least 8 sectors of the four heart sections. Sectors H, T and C corresponded to the infarct border zone, where the vectors were administered, while sector L was considered representative of the remote zone, since it was on the same plane but on the opposite position (posterior) relative to sector T. Each region was then divided into 2 pieces (for RNA analysis and histology, respectively) by a transversal cut in order to keep both the endocardial and pericardial borders visible in each piece. For all quantifications, the same regions were chosen in animals injected with either control or miR-199a vectors.

The protocol for the animal studies (n°76/2014 PR) was approved by the Italian Ministry of Health and was in accordance with the Italian law (D.lgs. 26/2014).

### LV assessment with cMRI

Cardiac magnetic resonance imaging was performed at 2 days and 4 weeks after MI. Animals were sedated with a cocktail of 4 mg/kg tiletamine hydrochloride and 4 mg/kg zolazepam hydrochloride injected intramuscularly and light anaesthesia was maintained by continuous intravenous infusion of propofol (30-40 mcg/kg/min) at spontaneous respiration. Pigs were placed in a right lateral position with the heart at the isocenter on MRI unit. ECG was monitored continuously.

cMRI images were acquired with a clinical 1.5 T scanner (Signa Excite HD; GE Medical Systems, Waukesha, WI, USA), using a non-breath-hold ECG gated, multi-NEX steady-state free precession pulse sequence (fast imaging employing steady-state acquisition) 32. The heart was scanned along two long axis views (vertical and horizontal) and with a set of short axis views covering the entire LV from atrioventricular valve plane to the apex. The following parameters were used: field of view 30 cm, slice thickness 8 mm, no gap between each slice, repetition time 3.7 msec, echo time 1.6 msec, views for segment 2, flip angle 45°, bandwidth 125 Hz, 30 phases, matrix 224 x 224, reconstruction matrix 256 x 256, NEX 3, free breathing. Myocardial oedema at 2 days post-MI was identified using T2-weighted short-tau inversion-recovery fast spin echo pulse sequence. The sequence parameters were field of view 30 cm; slice thickness: 8 mm, TR: 2 R-R intervals, TE: 100 ms, TI: 150 ms, matrix: 256 x 256 33. The main functional characteristics of pigs treated with either AAV6-Control or AAV6-miR-199a as detected by cMRI at different time points are summarised in Extended Data Table 1.

Tagging-cMRI images were acquired with an electrocardiography-gated, segmented K-space, fast gradient recalled echo pulse sequence with spatial modulation of magnetization to generate a grid tag pattern. Nonselective radiofrequency pulses separated by spatial modulation of magnetization-encoding gradients allowed tag separation of 10 mm. Three sets of short-axis at basal, middle and apical level views were acquired with a grid of tags line with 45° and 135° angulation. The number of views per phase was optimized based on heart rate. The following parameters were used: field of view 30 cm, slice thickness 8 mm,

no gap between each slice, repetition time 8 msec, echo time 4.3 msec, flip angle 15°, bandwidth 31 Hz, 30 phases, matrix 192 x 192, reconstruction matrix 256 x 256, NEX 3.

To identify the scar and quantify the extension of post-infarction fibrosis, delayed enhanced images were acquired in two-dimensional T1 weighted segmented inversion recovery gradient-echo-sequence 5-10 min after administration of gadoteric acid (Gd-DOTA 0.2 mmol/kg iv) in short- and long-axis views correspondent to those of cine-cMRI. The following parameters were used: field of view 30 mm, slice thickness 8 mm, no gap between each slice, repetition time 4.6 msec, echo time 1.3, flip angle 20°, matrix 224 x 192, reconstruction matrix 256 x 256, number of excitation 3.

Reveal (Medtronic) implantation involved a 2-cm cutaneous incision behind the left scapula. The device was inserted inside a subfascial pocket with the electrodes facing outward. Device data collection was activated by the programmer with R-wave sensing threshold of 0.12 mV to automatically detect arrhythmias. The parameters for episode detection were set as follows: FVT (interval 300 ms, duration 12/16 beats), VT (interval 360 ms, duration 16 beats), brady (interval 2000 ms, duration 4 beats), asystole (duration 3 sec) and AF (all episodes).

### **cMRI Image analysis**

Randomized images were analysed in a blinded manner under the supervision of a III-level EACVI (European Association of Cardiovascular Imaging) cardiac MRI accredited cardiologist, using commercially available research software package (Mass 6, Leyden, The Netherlands). In the acute phase of MI, the region corresponding to infarct-related oedema was defined based on a signal intensity 2 times higher than the mean SI of normal myocardium on T2 weighted short-axis images and the oedema size expressed as a percentage of total LV mass 33.

Global LV functional parameters (end-diastolic volume and end-systolic volume, ejection fraction) and left ventricular regional wall thickening (LVWT) were measured as previously described 20,34. LV endocardial and epicardial borders were manually traced on all short-axis cine images at the end-diastolic and end-systolic frames to determine the end-diastolic and end-systolic volumes, respectively, as well as ejection fraction and cardiac mass. The same software was used to calculate LVWT. Briefly, the middle slice (area of interest), orthogonal to LV long axis, at 30% of its length starting from the apex, was divided into 8 equal circumferential segments (Fig. 2f). The inferoseptal segment at the connection of the right ventricle with the left ventricle was defined as a reference point for the ventricular segmentation. Eight segments were plotted to generate the curve and subsequently calculate the area under the same curve (AUC) 19; Fig 2i).

The analysis of tagged cardiac images was performed using a custom software based on the method by Bogaert et al. 35 (cf. below Code availability). The two-dimensional maximal circumferential ( $E_{CC}$ ) and radial strain ( $E_{RR}$ ) were evaluated along short-axis LV slices, basal, middle, and apical, divided into 8 equal circumferential segments, starting from the reference point of the ventricular segmentation (Fig. 2f). The values for  $E_{CC}$  and  $E_{RR}$ , obtained for each segment, were plotted to generate curves, as in the case of LVWT (Fig. 2g



and 2h, respectively) and, subsequently, the AUC was calculated to integrate all the values along the LV circumference (scheme in Fig. 2i).

Myocardial regional perfusion was assessed with the first-pass technique 36. The first pass regional signal intensity/time curves, expressed as arbitrary unit/time, relative to different LV regions were generated using the Mass 6 software 37. Perfusion was evaluated semi-quantitatively with signal intensity/time curves by calculating the maximal upslope corresponding to the maximal signal intensity change during the wash-in phase for 18 segments obtained by sectioning the LV along three parallel short-axis planes, each divided in 6 segments.

To detect post-infarction fibrosis and determine its size, the LV short-axis stack of LGE images was first assessed visually for the presence of LGE. The quantification of LGE was then performed on all LGE-positive studies by manually adjusting a grey-scale threshold to define areas of visually identified LGE. These areas were then summed to generate a total volume of LGE and expressed as a proportion of total LV myocardium (%LGE; 38). The infarct areas were also analysed using the full width half maximum method 39 to differentiate the dense infarct core from the heterogeneous grey zone as previously described 20. The infarct core was defined as an area with SI > 50% of maximal SI of enhanced myocardium. The grey zone of the infarct periphery was defined as the myocardium with SI > peak of remote myocardium but <50% of maximal SI of the high SI myocardium. Finally, infarction core and the grey zone were quantified as a percentage of the total myocardium and as a percentage of the total infarct size.

### Code Availability

Tagged cardiac images were analysed using the custom software named "Tagging Tool", based on a previously described method 35. This software was implemented by the UOC Magnetic Resonance of Fondazione Toscana "G. Monasterio", Pisa, Italy. For any request to access to this software please contact GDA (email: [aquaro@ftgm.it](mailto:aquaro@ftgm.it)). This software is only for animal study and clinical use in humans is not permitted.

### DNA and RNA isolation and quantification

Total DNA was isolated using the DNeasy Blood & Tissue Kit (Qiagen) following the manufacturer's instruction and used as a template to detect and quantify vector DNA by real-time PCR. Primers and TaqMan® probe (Applied Biosystems, Foster City, CA, USA), recognising the CMV promoter driving miR-199a expression, were as described 11. The pig housekeeping 18S rRNA gene was used as a normalizer (ThermoFisher Scientific).

Total RNA, including the small RNA fraction, was isolated from pig tissue fragments using the miRNeasy Mini Kit (Qiagen) according to the manufacturer's instruction. DNase treatment was performed during RNA isolation according to the manufacturer's protocol. For gene expression analysis, total RNA was quantified by Nanodrop and reverse transcribed using hexameric random primers followed by qRT-PCR. The housekeeping GAPDH was used for normalization.

For miR-199a-3p quantification, total RNA was reverse transcribed using miRCURY LNA PCR synthesis kit (Exiqon) and qRT-PCR was performed with pre-designed miRCURY LNA PCR primer sets (Exiqon) and miRCURY LNA SYBR Green master mix according to the manufacturer's instructions. MicroRNA expression was normalized on the expression levels of 5S rRNA.

### Histological and immunofluorescence analyses

The hearts were briefly washed in PBS, weighted, sectioned as shown in Extended Data Figs. 2a and 2b, fixed in 10% formalin at room temperature, embedded in paraffin and further processed for histology or immunofluorescence. Haematoxylin–eosin and Masson's trichrome staining (Biotica) were performed according to standard procedure and analysed for morphology; extent of fibrosis was measured on 4x magnification images using Image J.

For immunostaining, pig heart sections were deparaffinized in xylene and rehydrated. Antigen retrieval was performed by boiling samples in sodium citrate solution (0.1 M, pH 6.0) for 20 min. Sections were let cool down and permeabilised for 20 min in 1% Triton X-100 in PBS, followed by blocking in 1% BSA (Roche). Sections were then stained overnight at 4°C with the following primary antibodies diluted in blocking solution, recognizing the following antigens: sarcomeric  $\alpha$ -actinin (Abcam), Ki67 (Cell Signaling), histone H3 phosphorylated at serine 10 (Millipore), Aurora B kinase (Abcam), GATA4 (Abcam), desmin (Roche), myogenin (Cell Marque), endothelin receptor B (Abcam), Wt1 (Cell Marque), CD34 (Roche), CD45 (Roche). Sections were washed with PBS and incubated for 2 h with the respective secondary antibodies conjugated with Alexa Fluor-488, -555 or -647 (Life Technologies). Nuclei were stained with Hoechst 33342 (Life Technologies). Alternatively, after endogenous peroxidase inhibition with 3% H<sub>2</sub>O<sub>2</sub>, sections were incubated with appropriate biotin-conjugate secondary antibody (Abcam) in TBS-BSA 1% for 1 h at room temperature. Following signal amplification with Avidin–Biotin-Complex-HRP (VECTASTAIN), DAB solution (VECTOR) was applied for 3 to 10 min. Hematoxylin (Biotica) was further used to stain nuclei.

For BrdU incorporation analysis, after section permeabilisation, DNA denaturation was obtained by incubating 10 min in 1M HCl on ice and 20 min in 2M HCl at 37°C. Sections were further incubated with 0.1 M sodium-borate buffer pH 8.4 for 12 min at room temperature, washed three times with PBS and then blocked for 1 h in 10% horse serum PBS. Tissue sections were stained overnight at 4°C with anti- $\alpha$ -actinin antibody (Abcam) in 5% horse serum PBS and in anti-BrdU (Abcam). Washes and secondary antibody incubation were performed as described above.

To measure CM cross sectional area, lectin Wheat Germ Agglutinin (WGA; Vector Labs) was diluted 1:100 in PBS and added with the secondary antibody to sample sections and incubated as described above. Capillary density was determined after staining histological sections with lectin Wheat Germ Agglutinin together with anti- $\alpha$ -SMA antibody (Sigma) diluted in PBS.

In all quantifications of immunofluorescence and immunohistochemistry images, we considered, for each animal, at least 8 sectors belonging to all four heart sections shown in

Extended Data Figs. 2a and 2b. For each region considered, histological analysis was performed by acquiring 7 high-resolution images at 20X magnification, which were quantified by blinded researchers.

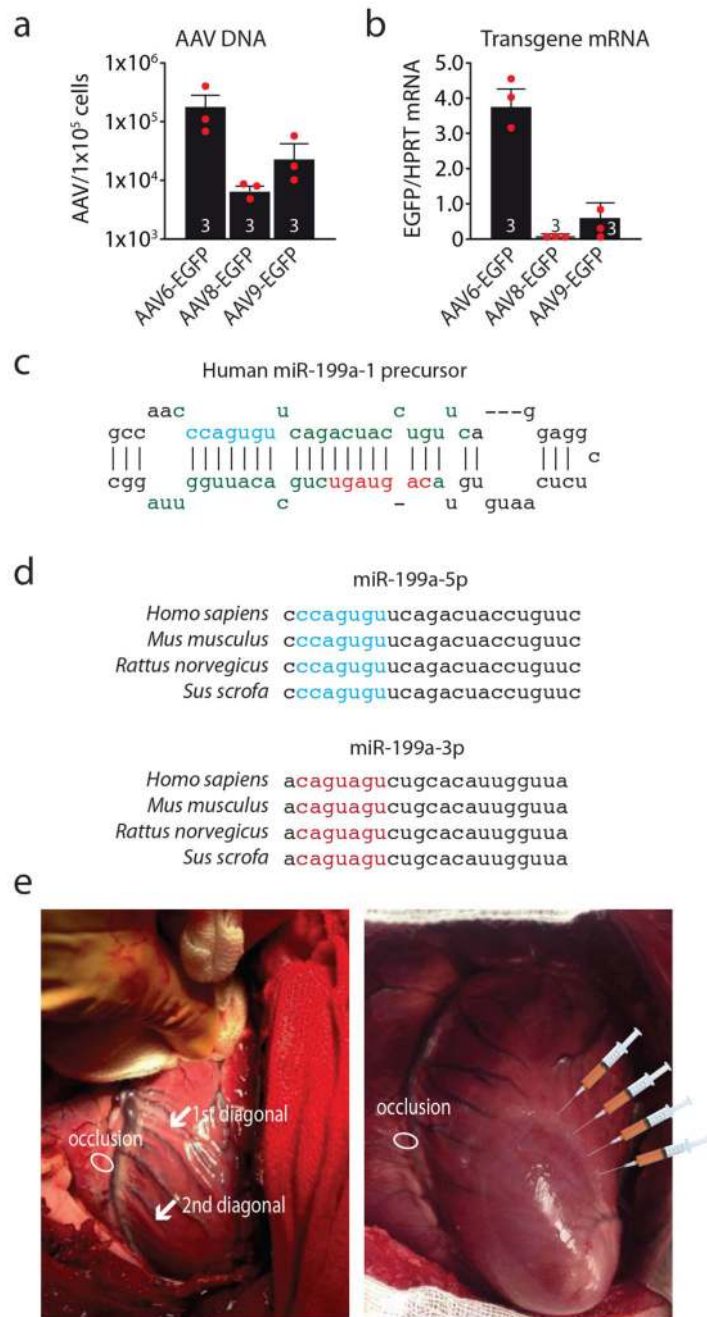
### **In situ hybridisation**

MicroRNA in situ hybridisation (ISH) was performed using locked nucleic acid (LNA) probes for miR-199a-3p and U6 snRNA, as well as an oligonucleotide with the same nucleotide content as the anti-miR-199a probe but in a scrambled sequence. Experiments were performed using a MicroRNA ISH kit for Formalin-fixed paraffin-embedded (FFPE) tissues (Qiagen) according to the manufacturer's protocol. Briefly, FFPE heart tissue slides were deparaffinised in xylene, treated with proteinase-K (15 µg/ml) for 10 min at 37°C and incubated with hsa-miR-199-3p (20 nM), scramble (20 nM) and U6 probes (2 nM) for one hour at 57°C in a hybridiser. After washing with SSC buffer, miRNA expression was detected using an anti-DIG alkaline phosphatase (AP) antibody (1:800) (Roche Diagnostics) supplemented with goat serum (Jackson Immunoresearch) and NBT-BCIP substrate (Roche Diagnostics).

### **Statistical analysis**

Data are presented as mean ± standard error of the mean (SEM). Statistical analysis was performed by employing commercially available software (GraphPad Prism). Data were first checked for normal distribution, then differences among groups were compared by one- and two-way ANOVA followed by the Bonferroni post-hoc test. Comparisons between 2 groups were made using the unpaired t-test. For survival analysis, a Kaplan-Meier survival curve was generated and log-rank statistics test was rendered. The AUC was obtained using the trapezoidal rule and statistical comparisons performed by one- and two-way ANOVA. For all the statistical analyses, significance was accepted at  $P < 0.05$ .

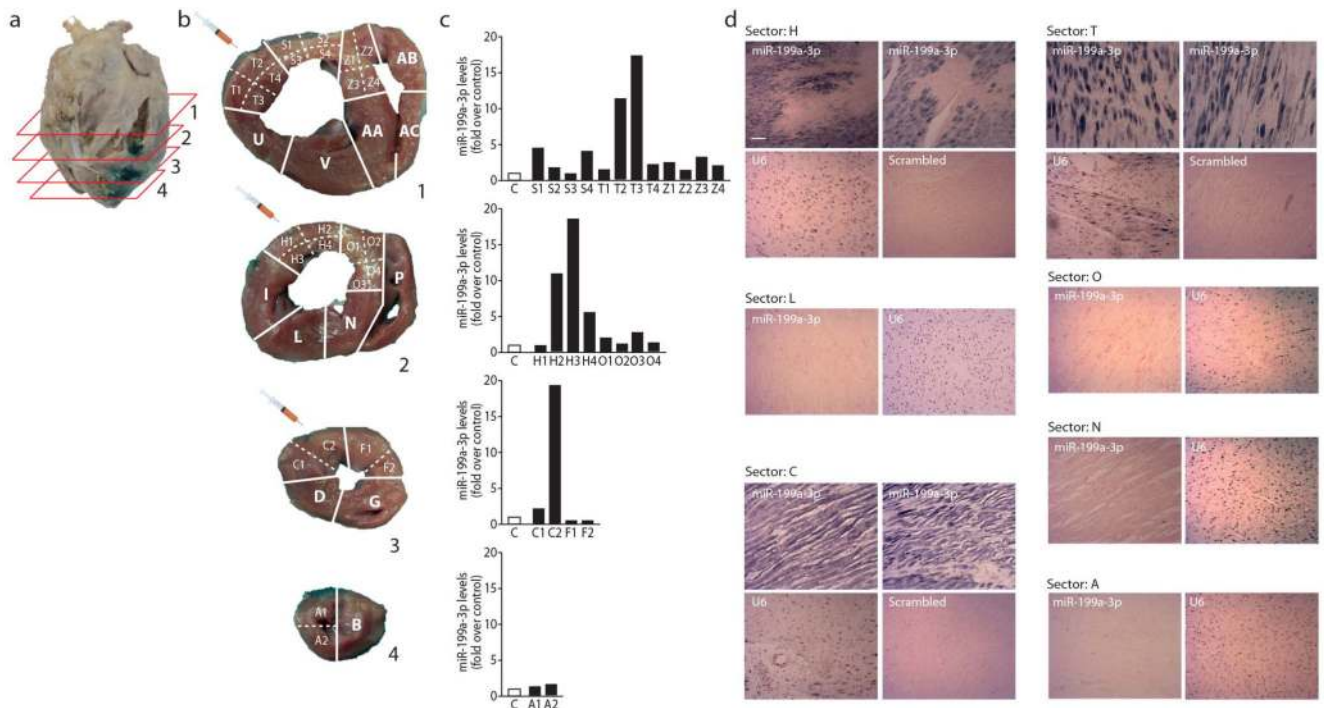
### **Extended Data**



**Extended Data Figure 1. Transduction of swine hearts after myocardial infarction with AAV vectors.**

**a-b**, Adeno-associated virus serotype 6 (AAV6) is the most effective serotype for porcine heart transduction. The graphs show viral genomes (a) and EGFP mRNA (b) levels one month after direct intramyocardial injection of  $1 \times 10^{12}$  v.g. particles of AAV6, AAV8 and AAV9 vectors carrying the EGFP transgene (these three AAV serotypes have been reported to transduce post-mitotic tissues at high efficiency - reviewed in ref. 28). Data are mean  $\pm$ SEM; the number of animals per group is indicated. **c**, Nucleotide sequence of the

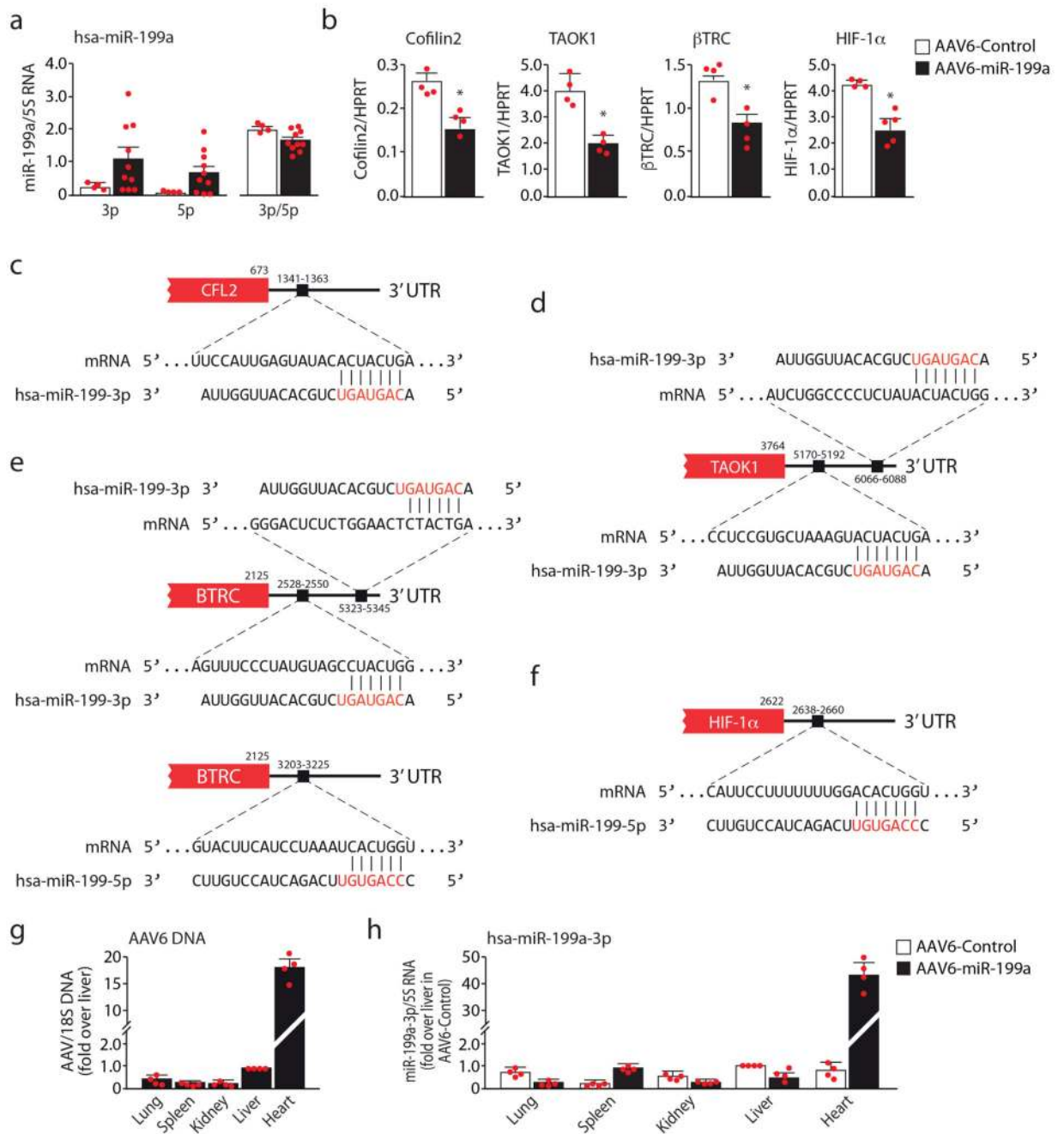
miR-199a-1 precursor. Mature miR-199a-5p and miR-199a-3p sequences are in green and their seed sequences are in blue and red respectively. **d**, Mature miR-199a-5p and miR-199a-3p sequences are conserved in human, mouse, rat and pig. The miRNA seed sequences are in blue for miR-199a-5p and in red for miR-199a-3p. **e**, Representative picture taken during porcine surgery and vector injection. After thoracotomy, the pericardial sac was opened, the LAD was exposed and occluded below its first branch for 90 minutes. Ten minutes after reperfusion, AAV6-Control or AAV6-miR-199a were injected into the infarct border zone.



**Extended Data Figure 2. Systematic assessment of miR-199a-3p expression after AAV6-mediated transduction.**

**a.** Schematic representation of pig heart sectioning for histological and molecular studies. After arrest in diastole, the heart was excised and the pericardial sac removed. AAV injection sites, which were marked with coloured epicardial sutures during surgery, were further traced with a green water-proof paint. Four 1-cm thick transversal slices were cut starting from the base to the apex (1 to 4 in the Figure). Each slice was subsequently divided into 2-8 regions, each one labelled with a capital letter, and then into additional sub-regions (letters plus numbers) for targeted molecular and histological analyses. Sectors H, T and C corresponded to the infarct border zone (BZ), where the vectors were administered, while sector L was considered representative of the remote zone. **b.** Injection and infarct border segments for each slice were divided into smaller fragments (dashed lines) to accurately assess the levels of expression of the transgene at 12 days after transduction. The syringe indicates the injection sites. **c.** For each slice and segment, the graphs show real-time PCR quantifications of the mature miR-199a-3p expressed as fold over endogenous levels (AAV6-Control). One representative animal is shown out of four analysed in the same systematic manner, with comparable results. **d.** In situ hybridisation of pig heart sections for the detection of miR-199a expression at the single cell level. Each of sectors indicated in panel b was tested by in situ hybridisation using locked nucleic acid (LNA) probes detecting miR-199a-3p or U6 snRNA, or a probe with the same nucleotide composition as the one against miR-199a-3p but with a scrambled sequence (scramble). Expression of miR-199a-3p was robust in cardiomyocytes and specific for the injected areas throughout the left ventricle. One representative animal is shown out of four analysed in the same systematic manner with comparable results. Scale bar: 100  $\mu$ m

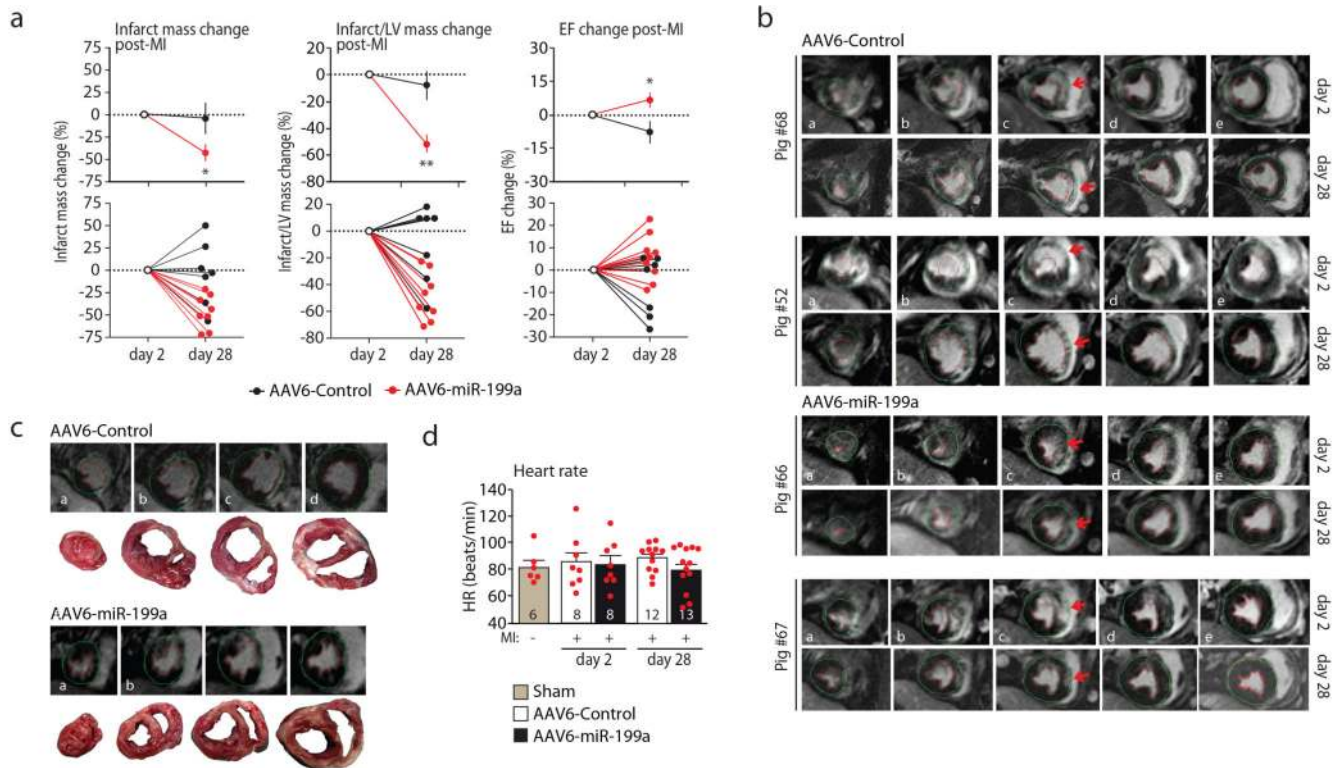




**Extended Data Figure 3. Downregulation of miR-199a target genes in transduced heart tissue and organ distribution of the AAV6-miR-199a vector.**

**a**, Real-time PCR quantification of both strands of miR-199a in AAV6-Control- and AAV6-miR-199a-injected pig hearts (n=4 and n=10 respectively) normalized over endogenous 5S rRNA. Data are mean $\pm$ SEM. **b**, mRNA levels of predicted and annotated target genes of miR-199a in AAV6-Control- and AAV6-miR-199a-treated pig hearts (n=4 per group) one month after MI and viral transduction. Data are mean $\pm$ SEM; \**P*<0.05 vs. AAV6-Control; t-test, two-sided. **c-e**, Predicted target sites of miR-199a-3p in the 3'UTR sequences of swine

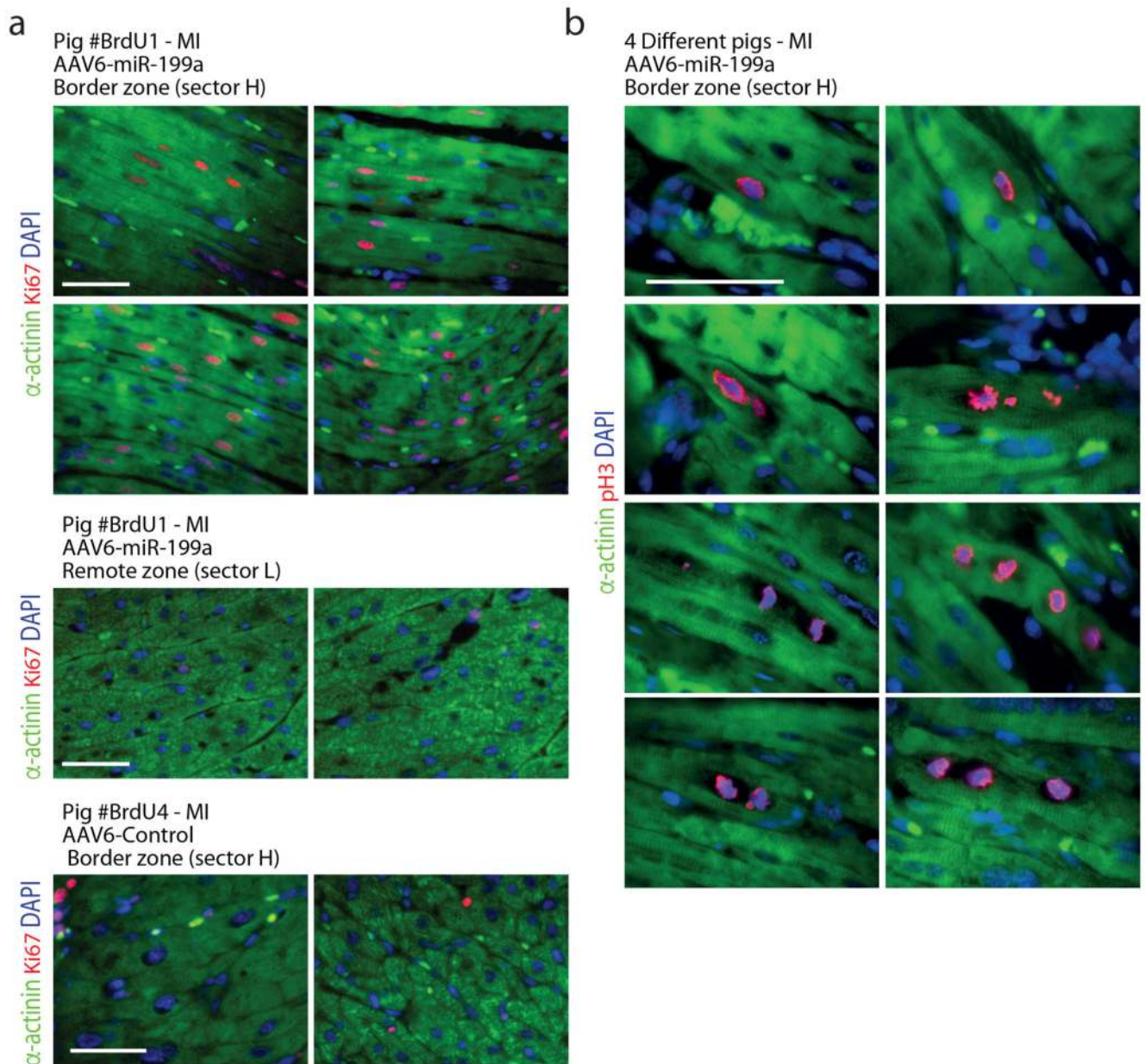
Cofilin2, TAOK1 and  $\beta$ TRC according to TargetScan Release 7.2. All these three genes are verified direct targets of this miRNA in rodents; the corresponding 3'UTR target sites for Cofilin2 and TAOK1 are conserved in swine; for  $\beta$ TRC, two alternative target sites in swine are shown. Other miR-199a-3p target genes originally identified in mice (in particular, Homer1 and Clic5 11,29) are not conserved in the swine genome. In the pig genome,  $\beta$ TRC also has an additional predicted target sequence for miR-199a-5p, which is indicated. **f.** Predicted target site of miR-199a-5p in the 3'UTR of pig HIF-1 $\alpha$  mRNA. **g.** Quantification of viral genomes in the indicated organs one month after intracardiac injection of AAV6-miR199a. Data are expressed as fold over liver levels after normalization for cellular DNA content using the 18S DNA as a reference (mean $\pm$ SEM, n=4 per group). The levels of viral DNA in myocardium of the injected animals were >18 times higher than in liver and >40 times higher than in other organs (spleen, kidney and lung). **h.** Levels of miR-199a-3p RNA in the indicated organs one month after intracardiac injection of AAV6-miR-199a. Data are shown as fold over endogenous miRNA levels in liver in control animals after normalization for cellular 5S rRNA (n=4 per group). Data are mean $\pm$ SEM. The amount of hsa-miR-199a-3p RNA was not elevated in any analysed organ, except for the heart. No overt signs of pathology, including hyper-proliferation (assessed by Ki67 staining) were observed.



**Extended Data Figure 4. MiR-199a improves global heart function and decreases infarct mass one month after treatment.**

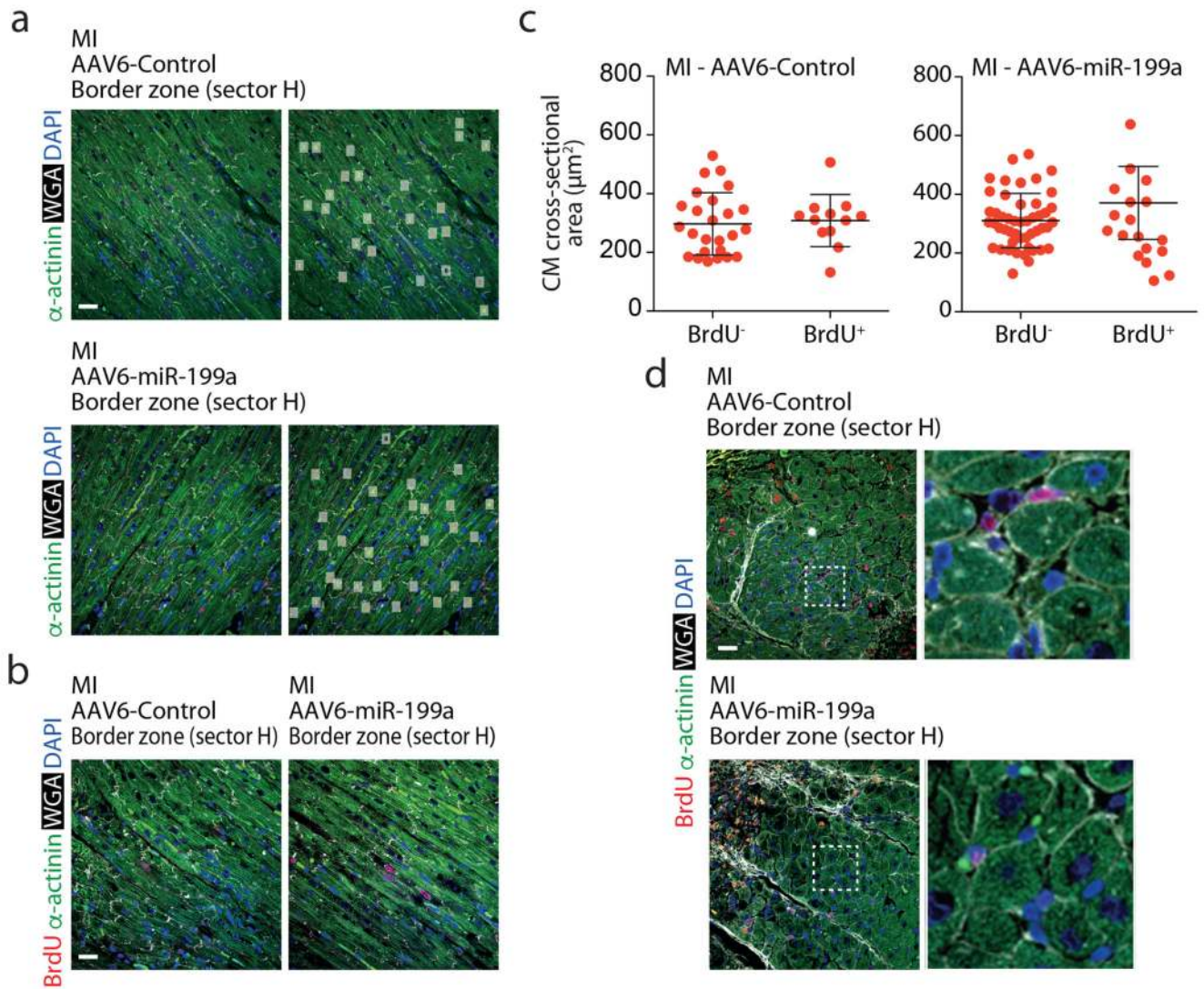
**a.** Graphs showing percent changes in infarct mass, infarct mass over LV mass and EF, as indicated, between 2 and 28 days after MI and AAV6-Control or AAV6-miR-199a delivery, measured by cMRI. The number of analysed animals were 7 and 8, 7 and 8, 7 and 9 for infarct mass, infarct mass over LV mass and EF for the two groups, respectively. Upper panels: cumulative values for all pigs. Data are mean±SEM; \**P*<0.05; t-test, two tailed; lower panels: data from individual pigs. **b.** Infarct healing at one month after AAV6-miR-199a injection. The LGE-cMRI images (from apex to base, a to e) are the same as in Fig. 1h without red counterstain. The red arrow shows the infarcted area in the central plane. **c.** Gross anatomy of cardiac slices with corresponding LGE-cMRI images in representative AAV6-Control and AAV6-miR-199a treated pig hearts, at 28 days post-MI. **d.** Heart rate in sham and infarcted animals injected with AAV6-Control and AAV6-miR-199a at one month after treatment. Data are mean±SEM; the number of animals per group and time point are indicated.





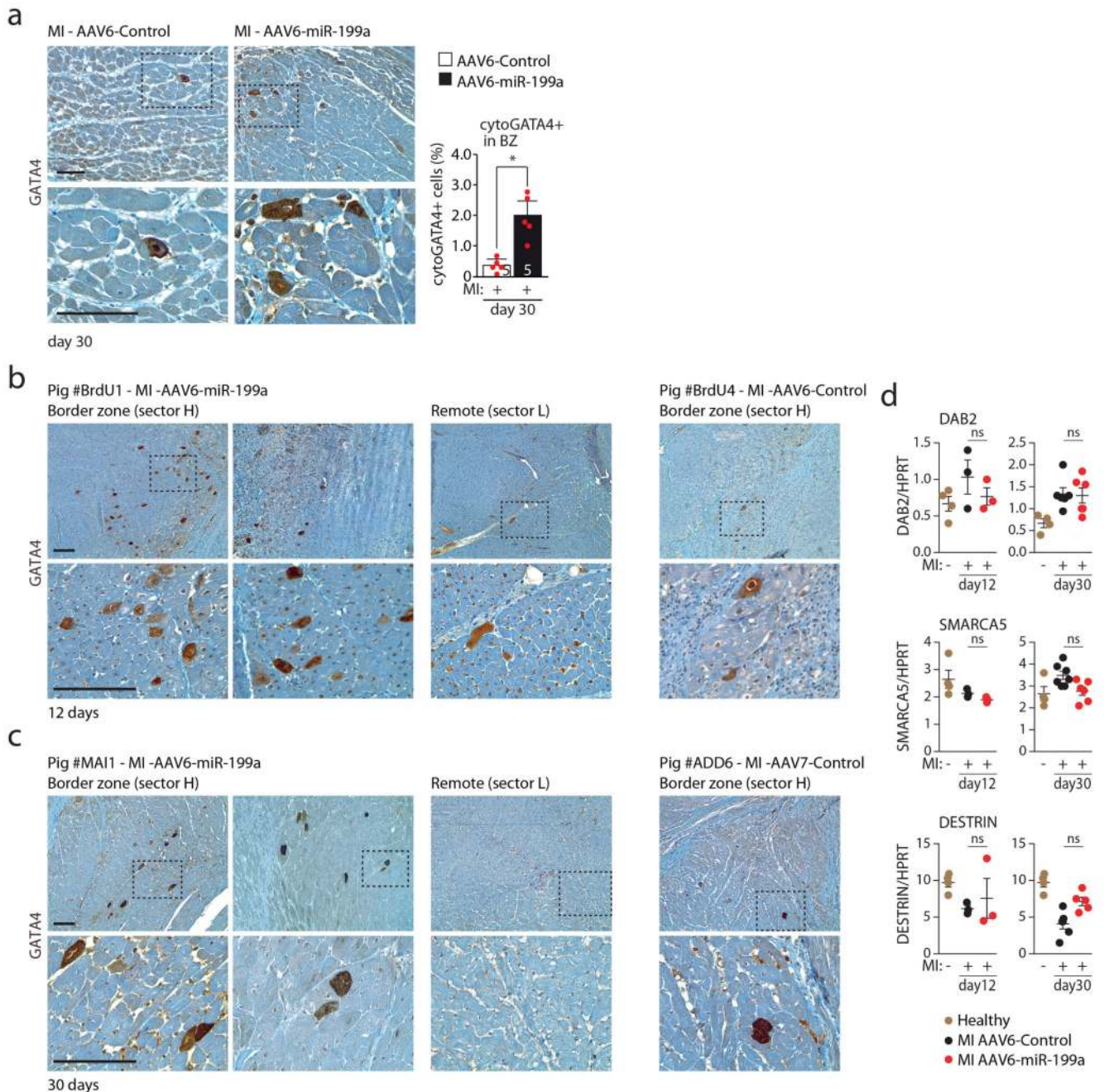
**Extended Data Figure 5. AAV6-miR-199a induces cardiomyocyte proliferation in vivo.**

**a**, Representative images of Ki67 and  $\alpha$ -actinin immunofluorescence staining of the infarct border (sector H) or remote (sector L) zones of AAV6-Control- and AAV6-miR-199a-treated animals (n=4 and n=6, respectively; analysis is from at least 7 high-resolution images acquired from at least 8 different regions of each heart), 12 days post MI. Scale bar: 100  $\mu$ m. At least 6 treated. **b**, High magnification representative images of phospho-histone H3 immunostaining in the infarct border zones of four different pigs treated with AAV6-miR-199a, 12 days post MI. Scale bar: 100  $\mu$ m.



**Extended Data Figure 6. Multinucleation and CM hypertrophy in miR-199a-treated pig hearts.**  
**a**, Representative images of longitudinal sections stained with wheat germ agglutinin (WGA) to assess the number of nuclei per CM in the infarct border zone of AAV6-Control- and AAV6-miR-199a-treated animals ( $n=4$  and  $n=6$ , respectively; analysis is from at least 7 high-resolution images acquired from at least 8 different regions of each heart), 12 days post MI. The right panels show the estimated number of nuclei for each cardiomyocyte. Scale bar: 50  $\mu\text{m}$ . **b**, Additional representative images of mono- or bi-nucleated BrdU-positive CMs in the infarct border zone of AAV6-Control- and AAV6-miR-199a-treated animals, 12 days post MI. Scale bar: 50  $\mu\text{m}$ . **c**, Cross-sectional area measurements of BrdU+ and BrdU- cardiomyocytes in AAV6-Control- and AAV6-miR-199a-treated pigs 12 days after surgery. Data are mean $\pm$ SEM from the analysis of 4 pigs. **d**, Representative images of BrdU+ and BrdU- CM. Scale bar: 50  $\mu\text{m}$ . The right panels are high magnification images of the indicated portions of the left images.



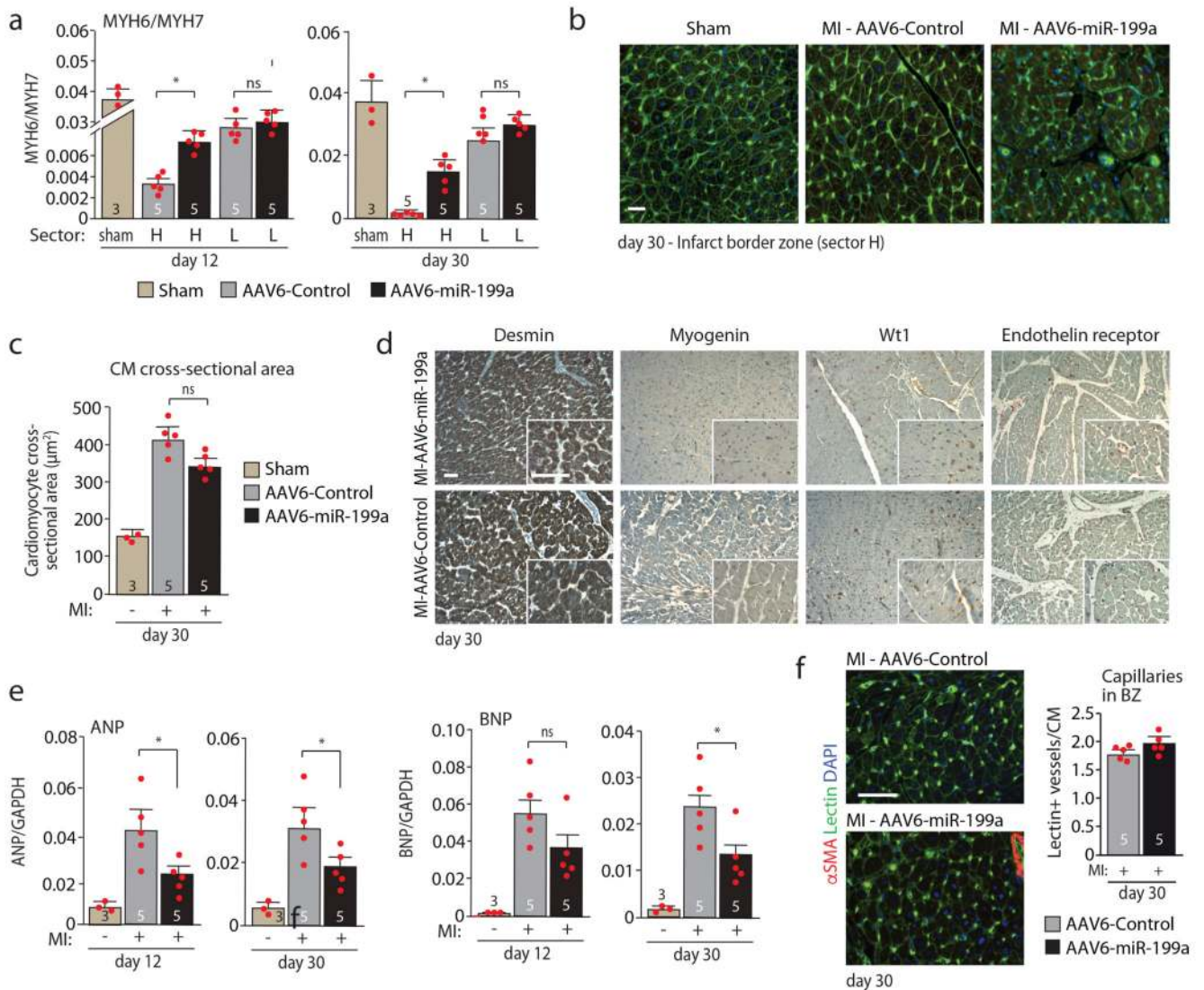


**Extended Data Figure 7. Expression of GATA4 in cardiomyocytes in the infarct border zone of AAV6-miR-199a-treated pigs.**

**a.** Representative immunohistochemistry images of GATA4-positive cells in AAV6-Control- and AAV6-miR-199a-injected pigs, 30 days after treatment. The bottom panels are high magnification images of the indicated portions of the upper images. The graph on the right shows quantification of cells showing GATA4 cytoplasmic localization. Data are mean  $\pm$ SEM; the number of animals per group is indicated. Quantification is from at least 7 high-resolution images acquired from at least 8 different regions of each heart. \* $P$ <0.05; t-test,



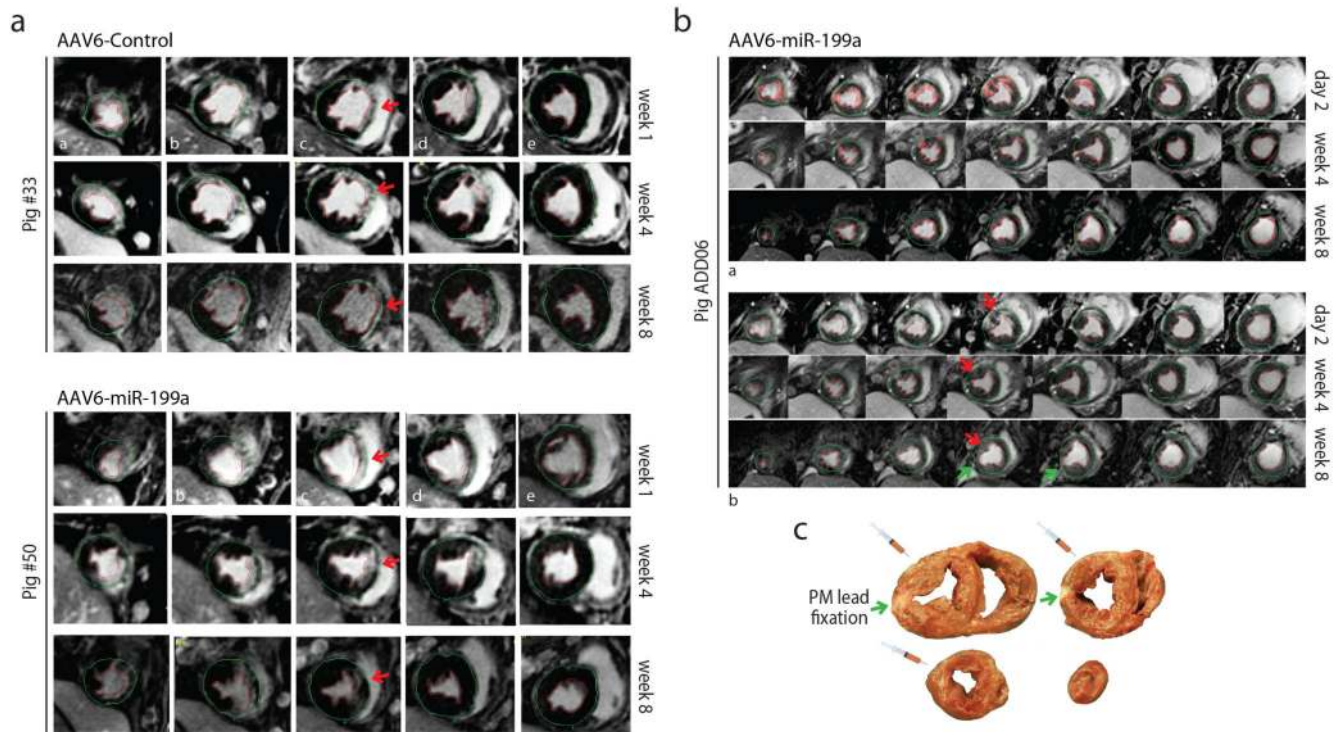
two sides. Scale bar: 100  $\mu\text{m}$ . **b-c.** Additional low and high magnification representative immunohistochemistry images of GATA4-positive cells in the infarct border (sector H) or remote zone (sector L) of AAV6-Control- and AAV6-miR-199a-injected pigs, 12 days (b) and 30 days (c) after treatment. Scale bar: 100  $\mu\text{m}$ . **d.** AAV6-miR-199a treatment does not alter the levels of DAB2, SMARCA5 and DESTRIN mRNAs. The graphs show real-time PCR quantifications of the levels of the indicated genes in sham, AAV6-Control- and AAV6-miR-199a-injected pig hearts, at 12 and 30 days after surgery; n=3 per group. Data are mean  $\pm$ SEM; the number of animals per group and time point is indicated. ns: not significant; \* $P$ <0.05 vs. AAV6-Control at the same time point, t-test, two-sided.



**Extended Data Figure 8. Molecular correlates of miR-199a transduction.**

**a**, Real-time PCR quantification of the ratio between  $\alpha$ - and  $\beta$ -myosin heavy chain mRNA in sham, AAV6-Control- and AAV6-miR-199a-injected pig hearts, at 12 and 30 days after surgery in the H (border zone) and L (remote zone) cardiac sectors. Data are mean $\pm$ SEM; the number of animals per group and time point is indicated. ns: not significant; \* $P$ <0.05 vs. AAV6-Control at the same time point; two-way ANOVA with Bonferroni post-hoc. **b,c**, Lectin immunofluorescence images (b) of sham, AAV6-Control- and AAV6-miR-199a-treated pig sections, 30 days after MI and vector administration along with quantification (c) of CM cross-sectional area ( $\mu\text{m}^2$ ). Data are mean $\pm$ SEM; the number of analysed animals is indicated. ns: not significant. One-way ANOVA with Bonferroni post-hoc. Scale bar: 50  $\mu\text{m}$ . **d**, Low and high magnification (insets) representative images of infarcted hearts injected with AAV6-Control or AAV6-miR-199a after immunohistochemistry to detect desmin (which is essential for maintaining structural and functional integrity of myocytes 40 and was expressed at normally high levels), myogenin (which coordinates skeletal myogenesis

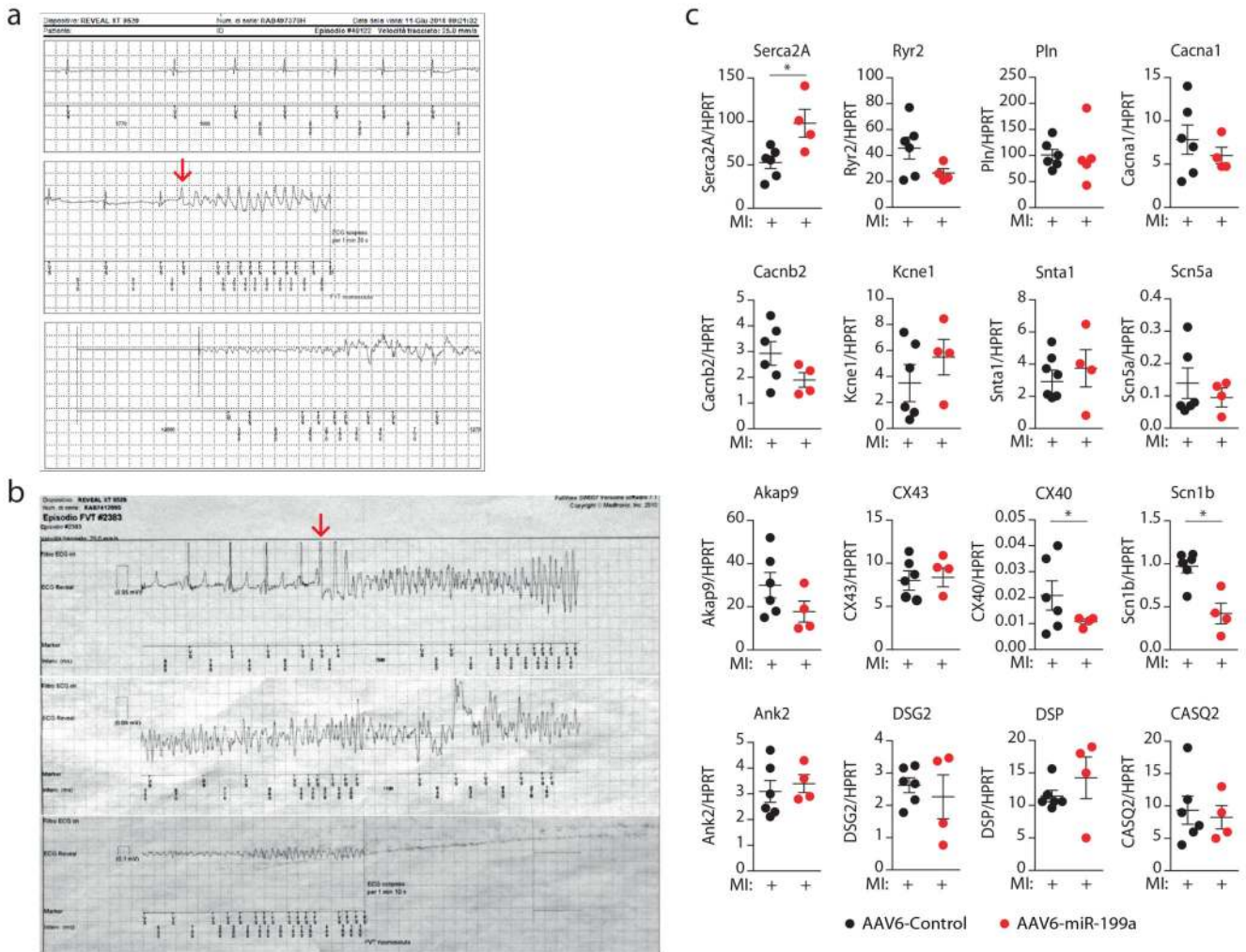
and repair 41 and was not expressed), endothelin-B receptor (which selectively stained arterioles smooth muscle cells) and Wilms' tumour protein 1 (Wt1, which was expressed at low levels in the vascular endothelium, but not in myocytes). Analysis was performed in at least 7 high-resolution images acquired from at least 8 different regions of the heart of 3 pigs per group. Scale bar: 100  $\mu\text{m}$ . **e**, Real-time PCR quantification of the levels of ANP and BNP in sham, AAV6-Control- and AAV6-miR-199a-injected pig hearts, at 12 and 30 days after surgery. Data are mean $\pm$ SEM; the number of animals per group and time point is indicated. ns: not significant; \* $P$ <0.05 vs. AAV6-Control at the same time point. One-way ANOVA with Bonferroni post-hoc. **f**, Representative sections of pig hearts treated with AAV6-Control and AAV6-miR-199a at day 30 after infarction and vector injection stained with FITC-lectin to visualize vessels and with an anti- $\alpha$ -SMA antibody to detect smooth muscle cells, along with quantification of lectin-positive vessels. No significant difference between the two MI groups was detected in capillary density at either 12 or 30 days. Data are mean $\pm$ SEM; the number of animals per group is indicated. Analysis was performed in at least 7 high-resolution images acquired from at least 8 different regions of the heart. \* $P$ <0.05. t-test, two-sided. Scale bar: 100  $\mu\text{m}$ .



**Extended Data Figure 9. Long-term expression of miR-199a induces progressive cardiac regeneration.**

**a**, The LGE-cMRI images (from apex to base, a to e) are the same as in Fig. 4a without red counterstain. The red arrow shows the infarcted area in the central plane c. **b**, cMRI images from a pig sacrificed at week 8 after MI and AAV6-miR-199a treatment. The upper panels show serial images from apex to base at day 2, week 4 and week 8; the infarct area is counterstained in red. The bottom panels show the same images without counterstaining. The green arrow shows the pacemaker lead attachment site. **c**, Gross anatomy of cardiac slices of the pig shown in panel b at sacrifice. The syringe indicates the injected area. The green arrow shows the pacemaker lead attachment site. Similar cardiac repair results were observed in three pigs treated with miR-199a that survived 2 months after treatment.



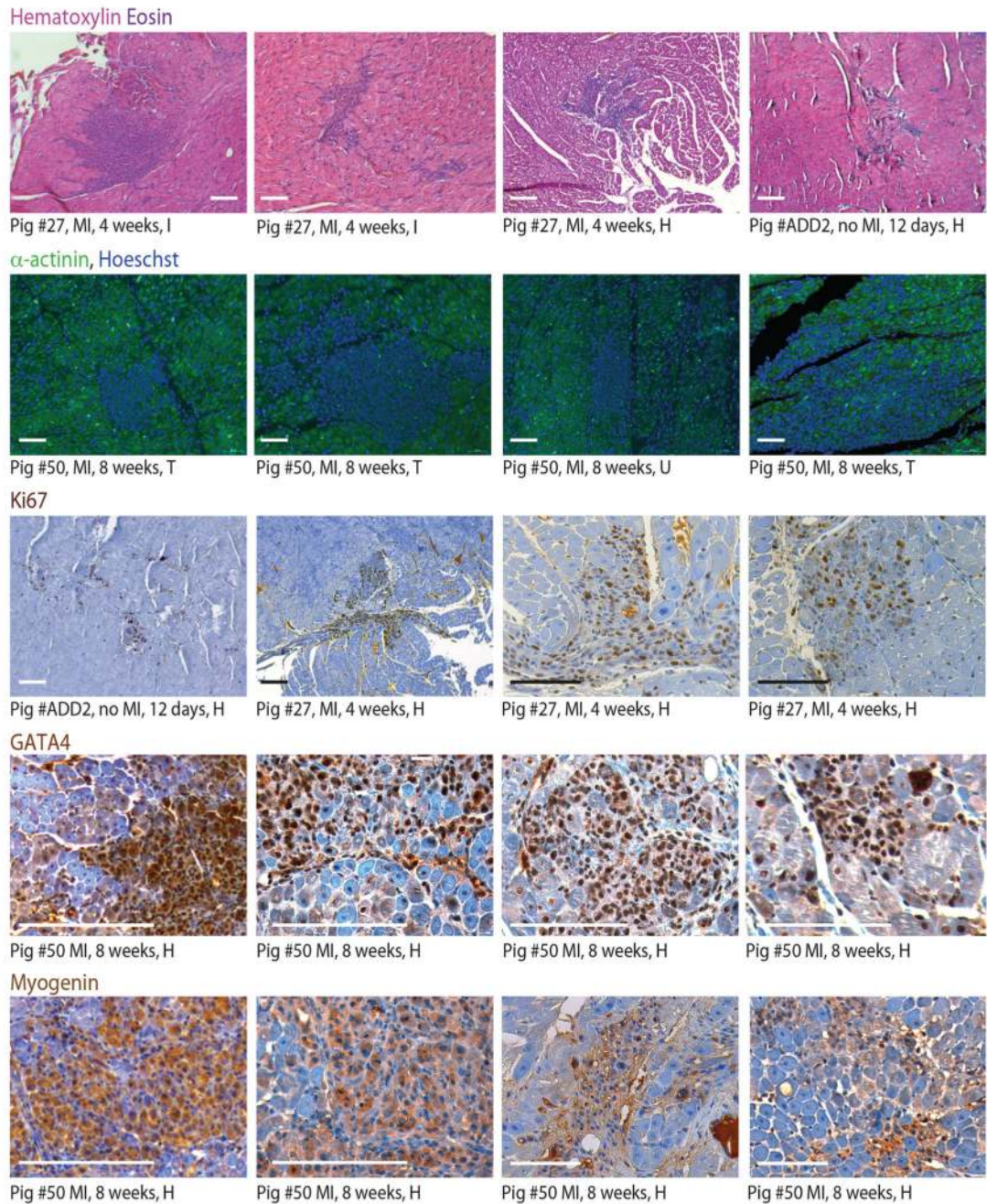


**Extended Data Figure 10. Recording of fatal arrhythmias in two infarcted pigs treated with AAV6-miR-199a-3p.**

Initiation of ventricular fibrillation recorded at the moment of death in two AAV6-miR-199a pigs by implanted miniaturized ECG recorders (Reveal, Medtronic, 9529). **a**, A premature ventricular ectopic beat (red arrow) with a coupling interval of 380 ms during a slowing heart rhythm induced a fast ventricular tachycardia that degenerated in ventricular fibrillation. **b**, A premature ventricular ectopic beat (red arrow) with coupling interval of 350 ms induced a fast ventricular tachycardia that quickly degenerated in ventricular fibrillation of different amplitudes resembling polymorphic ventricular tachycardia. **c**. AAV6-mediated, long-term expression of miR-199a did not affect the expression levels of ion channels or associated proteins involved in known arrhythmogenic conditions. In the infarct border zone of pigs treated with AAV6-Control or AAV6-miR-199a (n=6 and n=4 respectively) at 30 days after transduction, the expression levels of genes known to be involved in the pathogenesis of the Long QT Syndrome (Scn5a, Kcne1, Snta1, Akap9, Ank2), Brugada syndrome (Cacna1, Cacnb2, Scn1b), Carvajal syndrome (DSP), Arrhythmogenic Right Ventricular Cardiomyopathy (DSG2, DSP), Catecholaminergic Polymorphic Ventricular Tachycardia (CASQ2, Ryr2) were assessed. Additional investigated mRNAs were those

coding for Serca2A (which also served as a positive control since it is depressed during heart failure and was found increased in miR-199a-treated animals), phospholamban (Pln), Connexins 40 and 43 (CX40 and CX43 respectively). The miR-199a-treated pigs in which analysis was performed included one pig that survived at 8 weeks (pig 50) and three pigs with sudden death at 7 weeks (pigs 55, 66 and 67). Data are mean $\pm$ SEM. ns: not significant; \*P<0.05 vs. AAV6-Control. t-test, two sided.





**Extended Data Figure 11. miR-199a induces formation of proliferating cell clusters with an early myoblast phenotype infiltrating the pig myocardium.**

Additional images of cell clusters infiltrating the infarcted hearts injected with AAV6-miR-199a after hematoxylin-eosin staining or immunostaining to detect the indicated antigens. These cells scored negative for the leukocyte common antigen CD45 and for CD34 (excluding their immune, hematopoietic or endothelial origin) and were highly proliferating, as inferred from virtually complete positivity for Ki67. These cells also scored negative for markers of muscle differentiation, including desmin (identifying myogenic cells of cardiac, smooth and striated muscle), sarcomeric  $\alpha$ -actinin (which labels Z lines in the cardiac and

skeletal muscle sarcomere) and HHF35 (a monoclonal antibody recognizing muscle-specific  $\alpha$ - and  $\gamma$ -actin); cells were also negative for Wt1 (marking several malignancies and the epicardium). The infiltrating cells were positive for GATA4 (which is critical for proper mammalian cardiac development) and myogenin (the reactivation of which characterizes rhabdomyosarcoma cells) as well as the calmodulin-binding protein caldesmon (which regulates smooth muscle contraction and is expressed at high levels in leiomyoma and leiomyosarcoma) and the endothelin-B receptor, normally expressed in smooth muscle cells. The pig identity, treatment, time of analysis and cardiac sector from which the sample was taken are shown for each picture. Scale bar: 100  $\mu$ m. Clusters of cells were never detected in control-injected animals, however in one animal injected with AAV6-miR-199a in the absence of MI.

**Extended Data Table 1**  
**Table reporting pig heart functional and morphological parameters from cMRI analyses.**

Animals are divided according to treatment (AAV-Control and AAV-miR-199a) and day of analysis (Day 2 and day 28).

Day 2							
AAV6-Control	EDV (ml)	ESV (ml)	SV (ml)	EF (%)	scar(g)	LV mass (g)	scar (%)
1 Pig 43	39.65	14.87	25.00	63.05	9.00	47.90	18.79
2 Pig 46	62.20	24.00	38.20	61.41	13.06	57.72	22.63
3 Pig 51	65.36	23.94	41.42	63.37	12.57	48.27	26.04
4 Pig 52	57.32	20.78	36.54	63.74	14.92	63.39	23.53
5 Pig 68	58.00	21.80	36.20	62.41	7.94	50.59	15.69
6 ADD 03	61.11	19.45	41.66	68.17	5.10	52.03	9.80
7 ADD 07	71.18	27.92	43.26	60.77	23.40	69.56	33.64
8 ADD 13	70.82	27.15	43.67	61.66	13.82	70.67	19.56
Mean	60.70	22.49	38.24	63.07635	12.48	57.52	21.21
Day 28							
AAV6-Control	EDV (ml)	ESV (ml)	SV (ml)	EF (%)	scar(g)	LV mass (g)	scar (%)
1 Pig 43	62.77	21.15	41.62	66.30	13.51	60.86	22.20
2 Pig 46	72.17	29.50	42.67	59.12	13.24	68.00	19.47
3 Pig 51	77.02	25.55	51.47	66.83	11.67	54.61	21.37
4 Pig 52	94.63	50.26	44.37	46.89	15.23	59.11	25.77
5 Pig 68	61.10	22.10	39.00	63.83	10.05	58.48	17.19
6 ADD 03	67.89	21.45	46.44	68.40	2.2	53.04	4.15
7 ADD 07	97.79	48.35	49.44	50.58	14.89	68.57	21.72
8 ADD 13	119.94	61.37	58.57	48.83	13.43	62.68	21.43
9 Pig 25	128.42	80.03	48.39	37.68	19	63.45	29.94
10 Pig 29	82.07	41.35	40.72	49.62	23.94	79.30	30.19
11 Pig 33	96.77	55.17	41.60	42.99	18.6	99.78	18.64
12 Pig 34	96.08	44.04	52.04	54.16	5.72	70.96	8.06

Mean	88.05	41.70	46.36	54.60	13.46	66.57	20.01
<b>Day 2</b>							
AAV6-miR-199a	EDV (ml)	ESV (ml)	SV (ml)	EF (%)	scar(g)	LV mass (g)	scar (%)
1 Pig 54	69.15	30.59	38.56	55.76	18.52	54.19	34.18
2 Pig 55	60.10	28.37	31.73	52.79	10.38	59.96	17.32
3 Pig 66	64.18	20.71	43.46	67.72	14.17	58.66	24.16
4 Pig 67	73.17	23.98	49.19	67.23	10.62	61.15	17.37
5 Pig 69	49.40	17.02	32.38	65.55	14.76	51.21	28.82
6 ADD 05	70.20	19.74	50.68	72.19	7.21	53.59	13.45
7 ADD 06	57.64	20.56	37.07	64.31298	10.8	64.36	16.78
8 ADD 16	57.75	27.56	30.19	52.27706	16.08	63.7	25.24
Mean	62.70	23.57	39.16	62.23	12.82	58.35	22.16
<b>Day 28</b>							
AAV6-miR-199a	EDV (ml)	ESV (ml)	SV (ml)	EF (%)	scar(g)	LV mass (g)	scar (%)
1 Pig 54	76.00	33.85	42.15	55.46	12.35	61.35	20.13
2 Pig 55	97.16	34.15	63.01	64.85	8.20	63.73	12.87
3 Pig 66	65.81	18.7	47.11	71.58	3.98	51.4	7.74
4 Pig 67	85.44	23.48	61.96	72.52	6.00	64.00	9.37
5 Pig 69	68.98	26.73	42.25	61.25	7.21	57.80	12.47
6 ADD 05	72.00	18.34	53.66	74.53	3.49	64.64	5.40
7 ADD 06	66.42	19.96	46.46	69.95	3.20	66.20	4.83
8 ADD 16	92.67	48.51	44.16	47.65	11.72	60.02	19.53
9 Pig 21	62.92	16.76	46.16	73.36	4.88	69.40	7.03
10 Pig 26	80.43	29.84	50.59	62.90	6.60	65.39	10.09
11 Pig 27	92.40	32.99	59.41	64.30	5.99	59.70	10.03
12 Pig 32	78.44	33.29	45.15	57.56	11.40	69.50	16.40
13 Pig 50	76.83	25.15	51.68	67.26	5.24	55.78	9.39
Mean	78.12	27.83	50.29	64.86	6.95	62.226	11.18

## Acknowledgments

This work was supported by the European Research Council (ERC) [Advanced Grants 250124 and 787971] to MG; the Leducq Foundation Transatlantic Network of Excellence [grant 14CVD04] to MG; the Fondazione CRTrieste [Project CTC], Trieste, Italy and the Italian Ministry of Health [grant RF-2011-02348164 “CardioRigen”] to GS, FAR and MG. GP, IS and HA are supported by an ICGEB Arturo Falaschi pre-doctoral Fellowship. The authors are grateful to Marina Dapas and Michela Zotti from the ICGEB AAV Unit for AAV vector production.

## References

1. Roth GA, et al. Global, Regional, and National Burden of Cardiovascular Diseases for 10 Causes, 1990 to 2015. *J Am Coll Cardiol.* 2017; 70:1–25. [PubMed: 28527533]
2. Eschenhagen T, et al. Cardiomyocyte Regeneration: A Consensus Statement. *Circulation.* 2017; 136:680–686. [PubMed: 28684531]
3. Porrello ER, et al. Transient regenerative potential of the neonatal mouse heart. *Science.* 2011; 331:1078–1080. [PubMed: 21350179]

4. Oberpriller JO, Oberpriller JC. Response of the adult newt ventricle to injury. *J Exp Zool.* 1974; 187:249–253. [PubMed: 4813417]
5. Poss KD, Wilson LG, Keating MT. Heart regeneration in zebrafish. *Science.* 2002; 298:2188–2190. [PubMed: 12481136]
6. Jopling C, et al. Zebrafish heart regeneration occurs by cardiomyocyte dedifferentiation and proliferation. *Nature.* 2010; 464:606–609. [PubMed: 20336145]
7. Kikuchi K, et al. Primary contribution to zebrafish heart regeneration by *gata4(+)* cardiomyocytes. *Nature.* 2010; 464:601–605. [PubMed: 20336144]
8. Senyo SE, et al. Mammalian heart renewal by pre-existing cardiomyocytes. *Nature.* 2013; 493:433–436. [PubMed: 23222518]
9. Giacca M, Zacchigna S. Harnessing the microRNA pathway for cardiac regeneration. *J Mol Cell Cardiol.* 2015; 89:68–74. [PubMed: 26431632]
10. Diez-Cunado M, et al. miRNAs that Induce Human Cardiomyocyte Proliferation Converge on the Hippo Pathway. *Cell reports.* 2018; 23:2168–2174. [PubMed: 29768213]
11. Eulalio A, et al. Functional screening identifies miRNAs inducing cardiac regeneration. *Nature.* 2012; 492:376–381. [PubMed: 23222520]
12. Aguirre A, et al. In vivo activation of a conserved microRNA program induces mammalian heart regeneration. *Cell Stem Cell.* 2014; 15:589–604. [PubMed: 25517466]
13. Plouffe SW, et al. Characterization of Hippo Pathway Components by Gene Inactivation. *Mol Cell.* 2016; 64:993–1008. [PubMed: 27912098]
14. Poon CL, Lin JJ, Zhang X, Harvey KF. The sterile 20-like kinase Tao-1 controls tissue growth by regulating the Salvador-Warts-Hippo pathway. *Dev Cell.* 2011; 21:896–906. [PubMed: 22075148]
15. Zhao B, Li L, Tumaneng K, Wang CY, Guan KL. A coordinated phosphorylation by Lats and CK1 regulates YAP stability through SCF(beta-TRCP). *Genes Dev.* 2010; 24:72–85. [PubMed: 20048001]
16. Xue B, Robinson RC. Guardians of the actin monomer. *Eur J Cell Biol.* 2013; 92:316–332. [PubMed: 24268205]
17. Rane S, et al. Downregulation of miR-199a derepresses hypoxia-inducible factor-1alpha and Sirtuin 1 and recapitulates hypoxia preconditioning in cardiac myocytes. *Circ Res.* 2009; 104:879–886. [PubMed: 19265035]
18. Lindsey ML, et al. Guidelines for Experimental Models of Myocardial Ischemia and Infarction. *Am J Physiol Heart Circ Physiol.* 2018
19. Koch KC, et al. Myocardial viability assessment by endocardial electroanatomic mapping: comparison with metabolic imaging and functional recovery after coronary revascularization. *J Am Coll Cardiol.* 2001; 38:91–98. [PubMed: 11451302]
20. Simioniuc A, et al. Placental stem cells pre-treated with a hyaluronan mixed ester of butyric and retinoic acid to cure infarcted pig hearts: a multimodal study. *Cardiovasc Res.* 2011; 90:546–556. [PubMed: 21257613]
21. Grabner W, Pfitzer P. Number of nuclei in isolated myocardial cells of pigs. *Virchows Arch B Cell Pathol.* 1974; 15:279–294. [PubMed: 4135954]
22. Molkenin JD, Lin Q, Duncan SA, Olson EN. Requirement of the transcription factor GATA4 for heart tube formation and ventral morphogenesis. *Genes Dev.* 1997; 11:1061–1072. [PubMed: 9136933]
23. Chen D, et al. Dual function of the UNC-45b chaperone with myosin and GATA4 in cardiac development. *J Cell Sci.* 2012; 125:3893–3903. [PubMed: 22553207]
24. Zhang H, et al. Qiliqiangxin Attenuates Phenylephrine-Induced Cardiac Hypertrophy through Downregulation of MiR-199a-5p. *Cell Physiol Biochem.* 2016; 38:1743–1751. [PubMed: 27161004]
25. Song XW, et al. MicroRNAs are dynamically regulated in hypertrophic hearts, and miR-199a is essential for the maintenance of cell size in cardiomyocytes. *J Cell Physiol.* 2010; 225:437–443. [PubMed: 20458739]



26. el Azzouzi H, et al. The hypoxia-inducible microRNA cluster miR-199a approximately 214 targets myocardial PPARdelta and impairs mitochondrial fatty acid oxidation. *Cell Metab.* 2013; 18:341–354. [PubMed: 24011070]
27. Li Z, et al. miR-199a impairs autophagy and induces cardiac hypertrophy through mTOR activation. *Cell Death Differ.* 2017; 24:1205–1213. [PubMed: 26160071]
28. Zacchigna S, Zentilin L, Giacca M. Adeno-associated virus vectors as therapeutic and investigational tools in the cardiovascular system. *Circ Res.* 2014; 114:1827–1846. [PubMed: 24855205]
29. Lesizza P, et al. Single-Dose Intracardiac Injection of Pro-Regenerative MicroRNAs Improves Cardiac Function After Myocardial Infarction. *Circ Res.* 2017; 120:1298–1304. [PubMed: 28077443]
30. Ayuso E, et al. Manufacturing and characterization of a recombinant adeno-associated virus type 8 reference standard material. *Hum Gene Ther.* 2014; 25:977–987. [PubMed: 25275822]
31. Arsic N, et al. Vascular endothelial growth factor stimulates skeletal muscle regeneration in vivo. *Mol Ther.* 2004; 10:844–854. [PubMed: 15509502]
32. Slavin GS, Saranathan M. FIESTA-ET: high-resolution cardiac imaging using echo-planar steady-state free precession. *Magn Reson Med.* 2002; 48:934–941. [PubMed: 12465101]
33. Masci PG, et al. Myocardial salvage by CMR correlates with LV remodeling and early ST-segment resolution in acute myocardial infarction. *JACC Cardiovasc Imaging.* 2010; 3:45–51. [PubMed: 20129530]
34. Lionetti V, et al. Mismatch between uniform increase in cardiac glucose uptake and regional contractile dysfunction in pacing-induced heart failure. *Am J Physiol Heart Circ Physiol.* 2007; 293:H2747–2756. [PubMed: 17704291]
35. Bogaert J, Rademakers FE. Regional nonuniformity of normal adult human left ventricle. *Am J Physiol Heart Circ Physiol.* 2001; 280:H610–620. [PubMed: 11158958]
36. Atkinson DJ, Burstein D, Edelman RR. First-pass cardiac perfusion: evaluation with ultrafast MR imaging. *Radiology.* 1990; 174:757–762. [PubMed: 2305058]
37. Positano V, et al. Myocardial perfusion by first pass contrast magnetic resonance: a robust method for quantitative regional assessment of perfusion reserve index. *Heart.* 2006; 92:689–690. [PubMed: 16614289]
38. Chan RH, et al. Prognostic value of quantitative contrast-enhanced cardiovascular magnetic resonance for the evaluation of sudden death risk in patients with hypertrophic cardiomyopathy. *Circulation.* 2014; 130:484–495. [PubMed: 25092278]
39. Schmidt A, et al. Infarct tissue heterogeneity by magnetic resonance imaging identifies enhanced cardiac arrhythmia susceptibility in patients with left ventricular dysfunction. *Circulation.* 2007; 115:2006–2014. [PubMed: 17389270]
40. Li Z, et al. Desmin is essential for the tensile strength and integrity of myofibrils but not for myogenic commitment, differentiation, and fusion of skeletal muscle. *J Cell Biol.* 1997; 139:129–144. [PubMed: 9314534]
41. Zammit PS. Function of the myogenic regulatory factors Myf5, MyoD, Myogenin and MRF4 in skeletal muscle, satellite cells and regenerative myogenesis. *Semin Cell Dev Biol.* 2017; 72:19–32. [PubMed: 29127046]



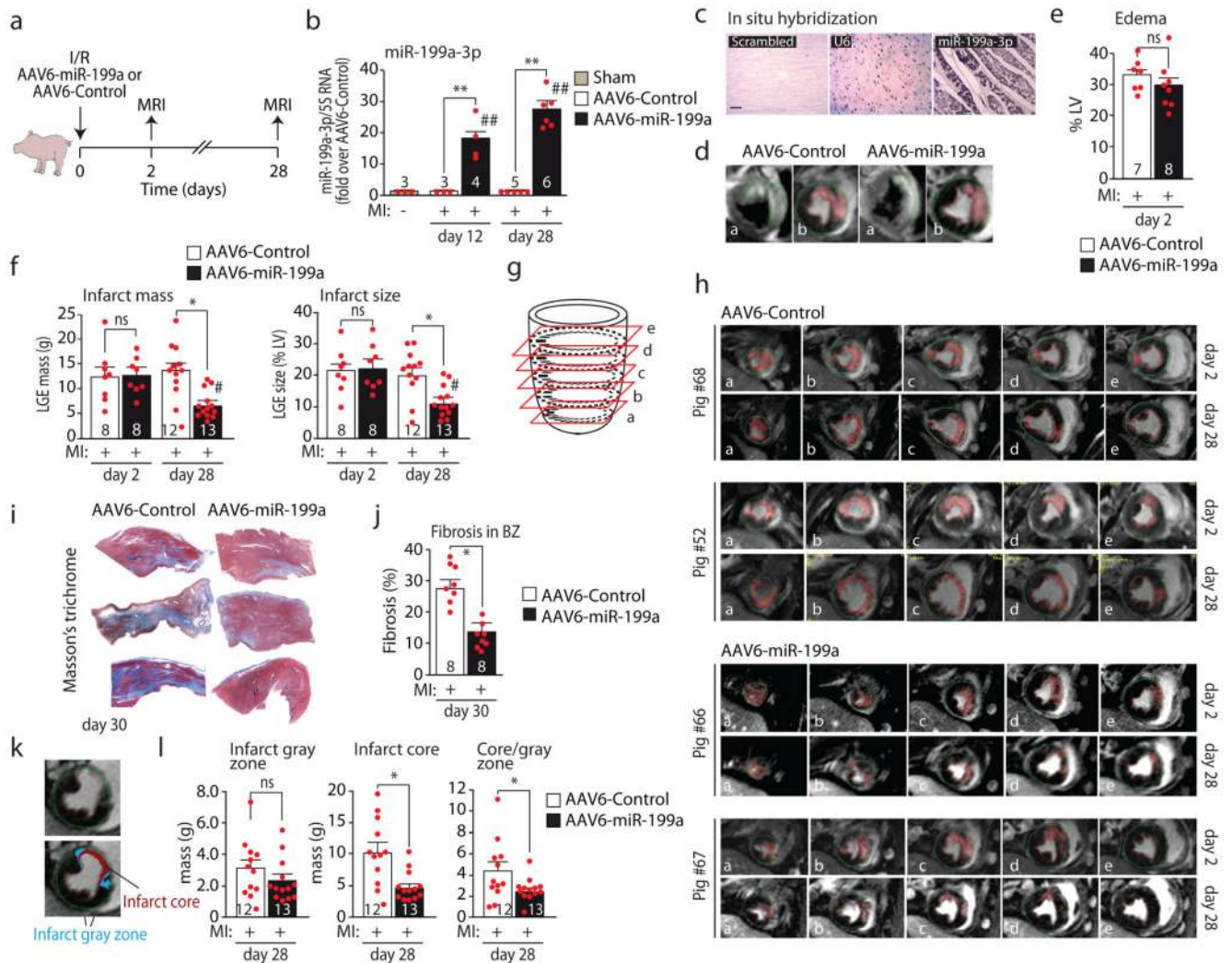


**Figure 1. miR-199a treatment reduces infarct size.**

**a**, Experimental protocol. **b**, Graph representing miR-199a-3p quantification 12 and 28 days after infarction and vector delivery. Data are represented as fold over endogenous levels (AAV6-Control) and expressed as mean±SEM; the number of animals per group and time point is indicated. \*\* $P < 0.01$  vs. AAV6-Control at the same time point; ### $P < 0.01$  vs. sham; two-way ANOVA with Bonferroni post-hoc. **c**, In situ hybridisation of miR-199a-3p, scrambled oligonucleotide and U6 LNA probes in pig heart sections at day 12 after treatment. Scale bar: 100  $\mu$ m. Analysis was performed in 8 different sectors of at least 5 animals per group as shown in Extended Data Fig. 2d. **d**, Examples of T2-weighted cMRI images showing cardiac oedema (a), with corresponding late gadolinium enhancement (LGE) cMRI images (b) at day 2 post-MI. Dark myocardium is viable, infarcted area is highlighted in red for better visualization. The number of analysed animals is indicated in panel e. **e**, Oedema (%LV) at two days after MI. Data are mean±SEM. ns: not significant; t-test, two-sided. **f**, LGE mass (g) and size (%LV), at days 2 and 28 post-MI. Data are mean ±SEM. ns: not significant; \* $P < 0.05$  vs. AAV6-Control at the same time point; # $P < 0.05$  vs.

AAV6-miR-199a at day 2 post MI; two-way ANOVA with Bonferroni post-hoc. **g**, Schematic representation of cMRI slices, from apex to base (a to e). **h**, LGE-cMRI images (from apex to base, a to e) of four representative pig hearts, two receiving AAV6-Control and other two AAV6-miR-199a at 2 and 28 days after MI. The infarct area is counterstained in red; the corresponding original images without counterstaining are shown in Extended Data Fig. 4b. The number of analysed animals is indicated in panel f. **i,j**, Masson's trichrome staining representative images of transverse heart sections of three treated and control pig hearts one month after surgery (i), with relative quantification of the area of fibrosis (j). Quantification is from at least 8 different regions of each heart, 8 animals per group. Data are mean±SEM. \* $P<0.05$ . t-test, two-sided. BZ: border zone. **k**, Identification of infarct scar and grey zone by LGE-cMRI. The number of analysed animals is indicated in panel l. **l**, Infarct grey zone, infarct core and their ratio 28 days post-MI measured by LGE-cMRI. Data are mean±SEM. ns: not significant; \* $P<0.05$  vs. AAV6-Control at the same time point; t-test, two-sided.

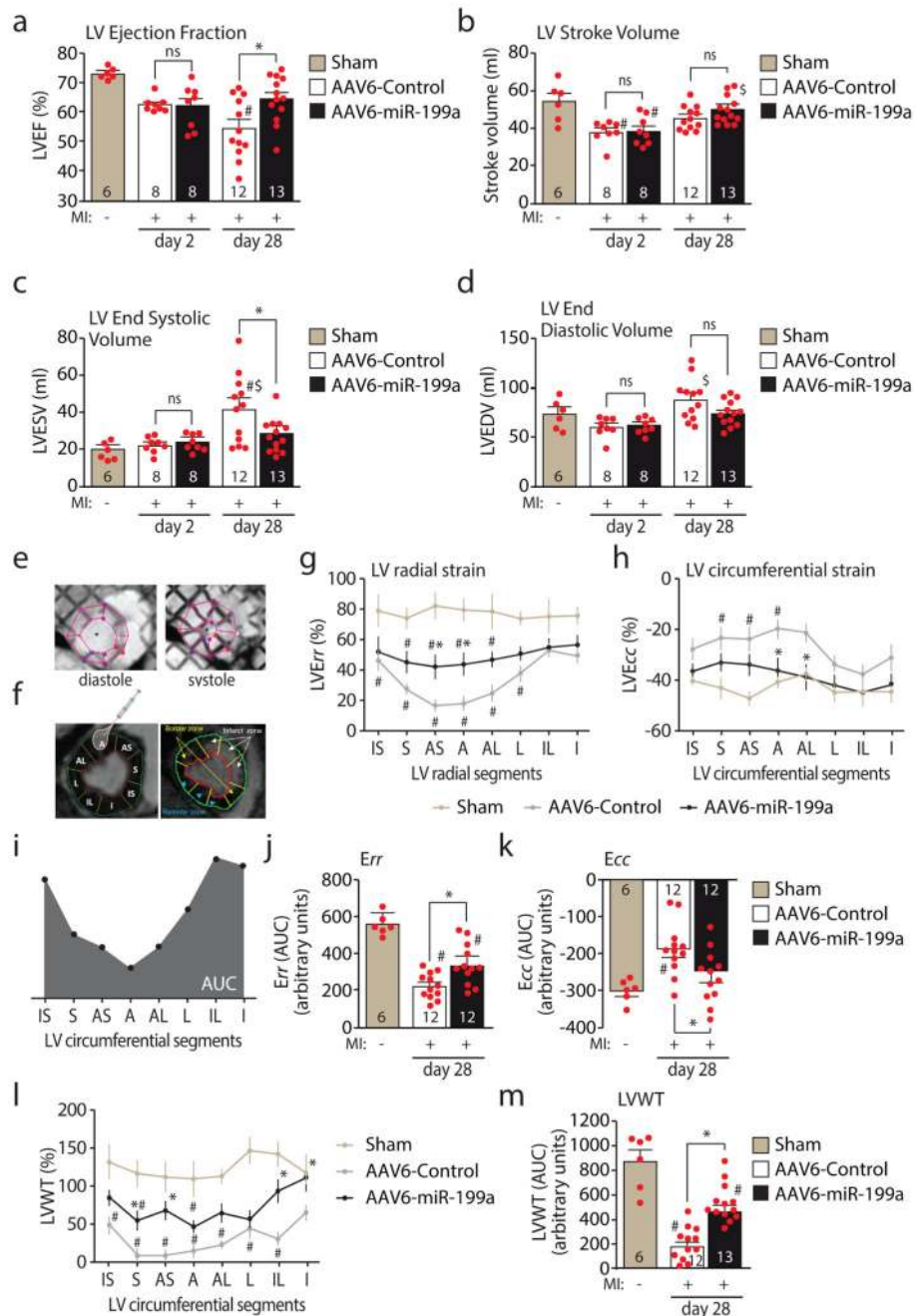


**Figure 2. miR-199a delivery improves global and regional cardiac function.**

**a-d**, LV ejection fraction (EF, %), stroke volume (ml), LV end-systolic volume (ml) and LV end-diastolic volume (ml) measured by cMRI in non-infarcted controls and infarcted animals at days 2 and 28 post-MI and either AAV6-Control or AAV6-miR-199a injection. Data are mean±SEM; the number of animals per group and time point is indicated. ns: not significant; \* $P < 0.05$  vs. AAV6-Control at the same time point; # $P < 0.05$  vs. sham; \$ $P < 0.05$  vs. day 2; two-way ANOVA with Bonferroni post-hoc. **e**, Example of cardiac short axis image with the tagging grid in diastole and systole. **f**, Subdivision of the LV short axis in 8

circumferential segments (left) and their correspondence with the infarct core, border zone and the remote zone (right). The syringe indicates the infarct border injected with AAVs. IS, inferoseptal; S, septal, AS, antero-septal; A, anterior; AL, anterolateral; L, lateral; IL, inferolateral; I, inferior. **g, h**, Eight-segment curves corresponding to LV radial (LVE<sub>rr</sub>) (g) and circumferential (LVE<sub>cc</sub>) (h) strain at 28 days after MI. Data are mean±SEM. \**P*<0.05 vs. AAV6-Control; #*P*<0.05 vs. sham; two-way ANOVA with Bonferroni post-hoc. The number of animals for the analysis is indicated in panels j and k. **i**, Schematic example of calculation of the area under curve (AUC) in arbitrary units. **j, k**, AUC for Err (j) and Ecc (k). Data are mean±SEM; the number of animals per group is indicated. \**P*<0.05 vs. AAV6-Control; #*P*<0.05 vs. sham; one-way ANOVA with Bonferroni post-hoc. **l**, Eight-segment curves corresponding to LV end-systolic wall thickening (LVWT) at 28 days after MI. Data are mean±SEM. \**P*<0.05 vs. AAV6-Control; #*P*<0.05 vs. sham; two-way ANOVA with Bonferroni post-hoc. The number of analysed animals is shown in panel m. **m**, AUC for LVWT. Data are mean±SEM; the number of animals per group is indicated. \**P*<0.05 vs. AAV6-Control; #*P*<0.05 vs. sham; one-way ANOVA with Bonferroni post-hoc.



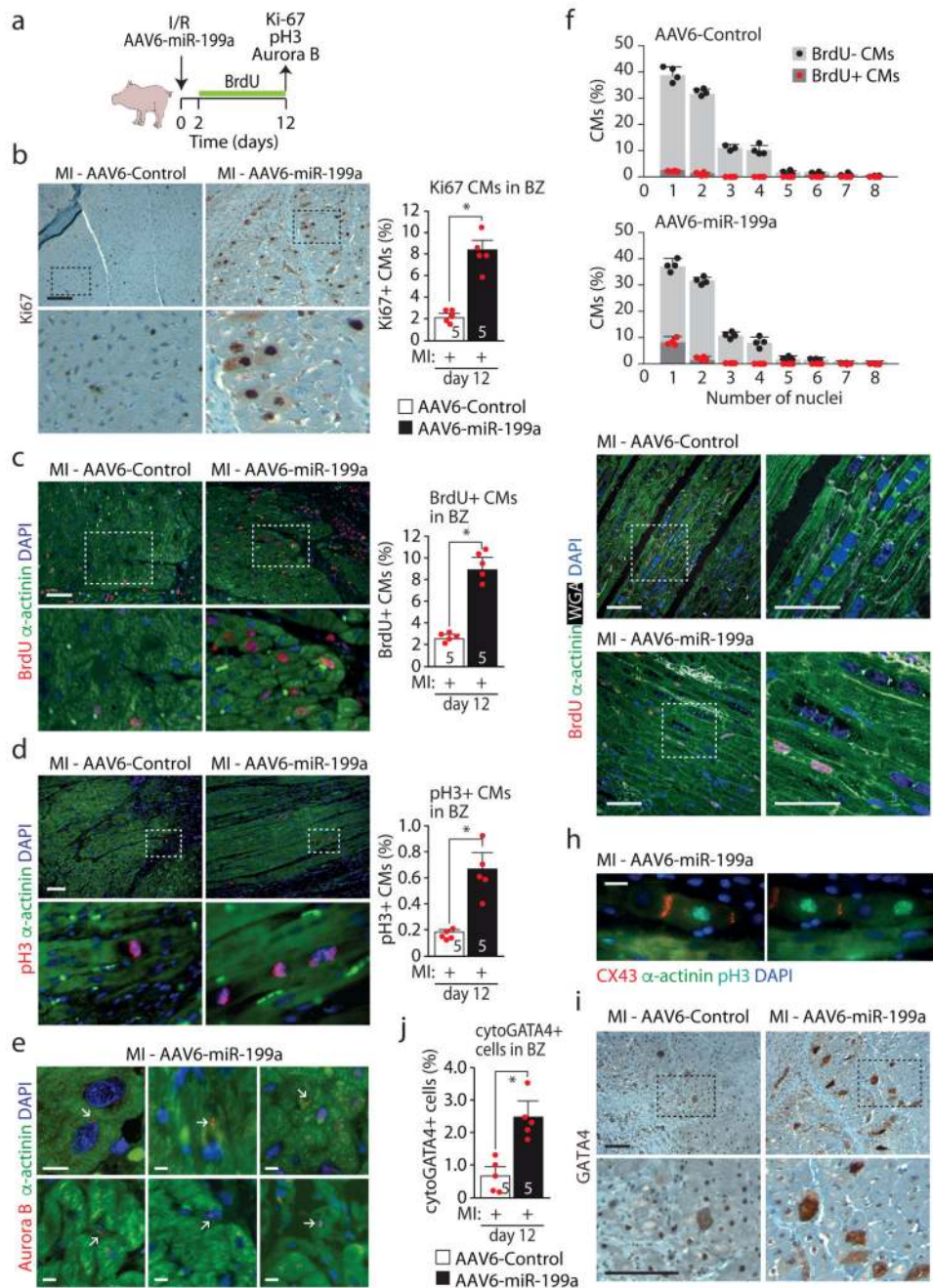


**Figure 3. AAV6-miR-199a administration induces cardiomyocyte proliferation.**

**a**, Schematic representation of the protocol for BrdU administration. **b**, Representative Ki67 immunohistochemistry images of the infarct border zone (BZ) 12 days after surgery, and relative quantification. The bottom panels are high magnification images of the indicated portions of the upper images. Data are mean±SEM; the number of animals per group is indicated. \**P*<0.05; t-test, two-sided. Scale bar: 100 μm. **c**, **d**, Representative images of BrdU (c) and phospho-histone H3 (d) immunostaining in the infarct border zone 12 days post MI, with relative quantifications. The bottom panels are high magnification images of

the indicated portion of the upper image. Data are mean $\pm$ SEM; the number of animals per group is indicated. \* $P$ <0.05; t-test, two-sided. Scale bar: 100  $\mu$ m. **e**, Aurora B immunofluorescence images showing localization in midbodies (arrow) in AAV6-miR-199a treated animals, 12 days post MI. Scale bar: 20  $\mu$ m. **f**, Distribution of the number of total and BrdU+ nuclei per CM in AAV6-Control- and AAV6-miR-199a-treated pigs 12 days after surgery. Data are mean $\pm$ SEM of four pigs with at least 8 sections analysed per pig. **g**, Representative images of multinucleated CMs with BrdU+ nuclei. WGA: wheat germ agglutinin to stain CM sarcolemma. Scale bar: 100  $\mu$ m. **h**, Connexin-43 (CX43, red) and phospho-histone H3 (pH3, blue-green) immunofluorescence representative images of AAV6-miR-199a-treated pig heart sections, 12 days after infarction. Scale bar: 100  $\mu$ m. **i**, Representative immunohistochemistry images of GATA4-positive cells in AAV6-Control- and AAV6-miR-199a-injected pigs, 12 days after treatment. The bottom panels are high magnification images of the indicated portions of the upper images. **j**, quantification of cells showing GATA4 cytoplasmic localization. Data are mean $\pm$ SEM; the number of animals per group is indicated. Quantification is from at least 7 high-resolution images acquired from at least 8 different regions of each heart. \* $P$ <0.05; t-test, two-sided. Scale bar: 100  $\mu$ m.

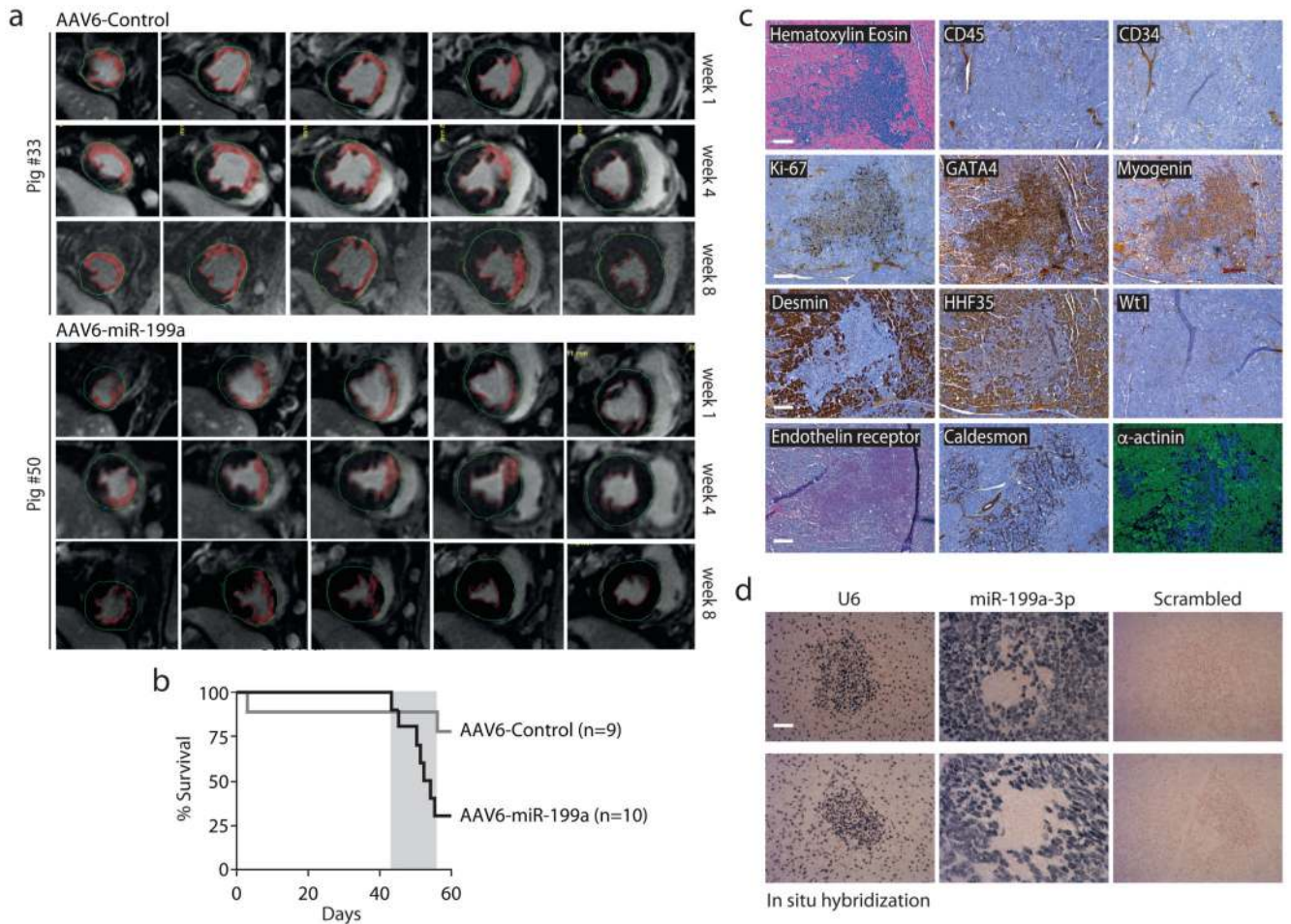


**Figure 4. Long-term expression of miR-199a induces progressive cardiac regeneration but causes sudden death.**

**a**, LGE-cMRI representative images, from apex to base, of one AAV6-Control and one AAV6-miR-199a-treated pig heart at 1, 4 and 8 weeks after MI. The infarct area is counterstained in red; the corresponding original images without counterstaining are shown in Extended Data Fig. 9a. Similar cardiac repair results were observed in three pigs treated with miR-199a that survived 2 months after treatment. **b**, Kaplan Meier curve (log-rank test) showing mortality after MI and vector administration. The number of animals per group is indicated. **c**, Hematoxylin-eosin staining or immunostaining for the indicated antigens of the same cell cluster in consecutive tissue sections from an infarcted heart injected with AAV6-miR-199a at 8 weeks after treatment. Scale bar: 100  $\mu$ m. **d**, In situ hybridisation of miR-199a-3p, scrambled and U6 LNA probes in pig heart sections with infiltrating cell cluster. Scale bar: 100  $\mu$ m.